

Determining and predicting the optical constants  $n$  and  $k$  for  
interstellar H<sub>2</sub>O:CH<sub>4</sub> ice mixtures

*Author:*

Coen Fransen,  
Sackler lab for astrophysics,  
Leiden University

December 18, 2014

*Supervised by:*

Prof. dr. H. Linnartz  
Dr. J.-B Bossa

*Referee and co-referee:*

Dr. A.J. Lock  
Dr. D.D. Land

## Abstract

In this thesis the different aspects of acquiring the complex refractive index of interstellar ice analogues are treated. The ultimate aim of this work is to search for abilities to predict the infrared absorption spectra of these analogues. A key factor in these predictions is the optical influence of porosity of the ice layers, since the porosity acts as a catalyst in the formation of more complex molecules. This chapters of this thesis will treat the following subjects:

- An introduction to interstellar ice research, followed by the theory of the research approach.
- A brief description of the used HV-setup.
- The results of the measurements.

During the writing of this report, it has yet to be confirmed whether the method developed for predicting the optical constants  $n$  and  $k$  works; if so, with what accuracy. However, from absorption peaks only visible for a porous mixture and not for pure and non-porous ices it can be concluded that the porosity likely causes different absorption behaviour. Another possible indication of porosity is a change in shape or size of the known absorption peaks of the individual ice components. It is hoped that, once validated, the method described in this thesis will be able to predict spectra of ternary ice mixtures.

# Contents

<b>1</b>	<b>Introduction</b>	<b>2</b>
<b>2</b>	<b>Interstellar ice research</b>	<b>3</b>
2.1	Interstellar medium . . . . .	3
2.2	Infrared spectroscopy . . . . .	6
2.3	Deposition rate . . . . .	8
2.4	Optical constants . . . . .	10
<b>3</b>	<b>HV-setup</b>	<b>12</b>
3.1	Vacuum system . . . . .	12
3.2	Optical interferometry system . . . . .	13
3.3	Infrared spectroscopy system . . . . .	14
<b>4</b>	<b>Results</b>	<b>15</b>
4.1	Compact & pure CH <sub>4</sub> . . . . .	15
4.1.1	Deposition rate . . . . .	15
4.1.2	Measurements spectra & optical constants . . . . .	16
4.2	Compact & pure H <sub>2</sub> O . . . . .	18
4.2.1	Measurements spectra & optical constants . . . . .	18
4.3	Porous mixture H <sub>2</sub> O:CH <sub>4</sub> (2:1) . . . . .	20
4.3.1	Deposition rate . . . . .	20
4.3.2	Measurements spectra & optical constants . . . . .	20
<b>5</b>	<b>Conclusion</b>	<b>23</b>
	<b>Bibliography</b>	<b>24</b>
<b>A</b>	<b>Traineeship assignment description</b>	<b>26</b>
<b>B</b>	<b>Python programs</b>	<b>27</b>
B.1	Min-Max . . . . .	27
B.2	Sigma-calculator . . . . .	32
B.3	NK-calculator . . . . .	34
<b>C</b>	<b>Succeeding deposition spectra measurements</b>	<b>37</b>

# Chapter 1

## Introduction

The Sackler lab for Astrophysics at the Leiden Observatory, Leiden University simulates the harsh conditions found in space in a fully controlled environment. The laboratory focusses primarily on the spectroscopic properties of different molecules and reactions, both in the solid and the gas phase. The main aim is to support astronomers in interpreting their observations. In this report ice layers are grown on a cryogenic substrate in an high vacuum setup, simulating ice layer growth on dust particles in space. In addition the wavelength dependent optical constants in the mid-infrared are determined, from which the absorbance behaviour of the ice layers can be predicted.

Due to the harsh conditions in space (i.e., intense radiation, low temperatures and low densities), classical chemistry predicts that there would be no molecules. However, inside interstellar clouds dust particles offer surfaces on which gas can deposit. This facilitates the forming of complex organic molecules ( $\geq 6$  atoms). Furthermore, the dust particles on the outside of the interstellar clouds shield the particles in the centre from the intense molecule destroying radiation. This shielding effect prevents the detection of any light from the interstellar clouds in the ultraviolet and visible light range. However, when infrared spectroscopy is applied, the ice components of the ice layers can be determined. [1] However, the porosity in space is hard to determine from astronomical data. The purpose of this report is to search for the possibilities to quantify this, since porous ices provide surface area for the catalysis of reactions taking place on dust particles. For astronomers this can be used as a reference to compare their observations with. From these values the absolute band strength of the components can be determined, which is another useful tool for astronomers.

In this report an introduction to astrophysics and the relevance of interstellar ice research to astronomers is given. Following, the theory of the research approach. Both can be found in chapter 2. Consecutively, an overview of the used setup with the different components is given in chapter 3. The results of the measurements are discussed in chapter 4. At last, a conclusion can be found in chapter 5.

## Chapter 2

# Interstellar ice research

In this chapter a brief explanation of interstellar medium and ices and their relevance to astronomers is given. Consecutive the basics of infra-red spectroscopy are explained. At last a description of the used HV-set-up is presented.

### 2.1 Interstellar medium

The space between the stars and planets, so called interstellar medium (ISM), is not empty. ISM consists mostly of gas, with densities ranging from  $10^{-4}$  to above  $10^8$  particles  $\text{cm}^{-3}$ . In comparison, earth's atmosphere contains approximately  $10^{19}$  particles  $\text{cm}^{-3}$ . The temperature of the gas particles can be above  $10^8$  K [2]. However, where the density is higher, the temperature generally is lower. This is found in interstellar clouds (see Fig. 2.1). The colourful areas are due to ionized gasses at the upper levels of ISM temperature range. The dark areas are denser (and therefore colder), where the dust particles and carbon based molecules are located [1].



Figure 2.1: The Carina Nebula, an interstellar cloud at a distance of 7500 ly from earth.  $1 \text{ ly} = 9,5 \cdot 10^{15} \text{ m}$ , the distance light travels in vacuum in a year. Credit: ESA/NASA [4].

The dust particles consist primarily of amorphous carbonaceous and silicates. These materials only evaporate far above 1200 K, so the particles can be considered inert. The outer particles shield the inner ones from dissociating UV blackbody radiation from stars, by absorption or refraction. The shielding also lowers the temperature to a point where gasses deposit on the dust particles, forming ice layers. Once deposited, the dust particles offer a reservoir where gas particles can be stored and kept together longer than in a gas cloud. This enables chemical processes (i.e. forming of complex molecules) to take place in an environment which would otherwise be too harsh for those molecules to exist. Over time these icy dust particles can form into comets, stars and planets. The particles are one of the main ingredients of the lifecycle of stars (see Fig. 2.2) [1] [2]. Besides the forming of the star, the dust particles are also responsible for a substantial amount of the molecules found on planets. The recent landing mission Rosetta on comet 67P/ChuryumovGerasimenko, aims at researching the composition of the comet. It was suspected that the comet consists mostly of water, which would be proof for the theory that earth's water comes from outer space i.e. comets. [5] However, results have shown a three times bigger higher amount of deuterium in the comet, compared to hydrogen. [3] Nonetheless theories like the presence of the building blocks of life (amino acids) on comets and their formation inside interstellar clouds are still deemed valid and are investigated. [6]

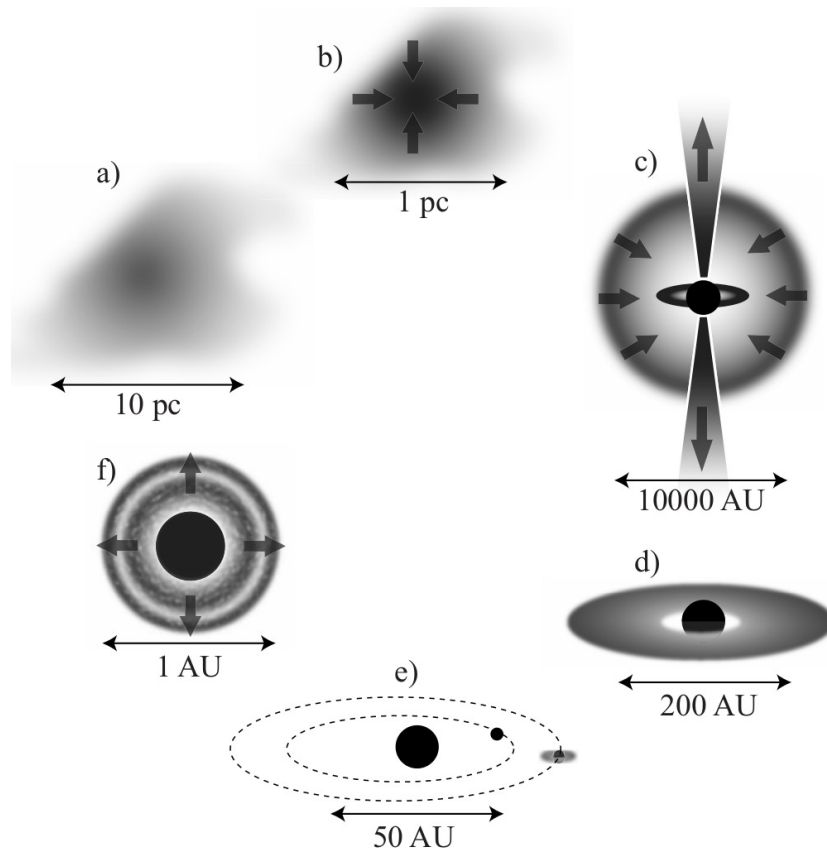


Figure 2.2: The lifecycle of a star, starting with a diffuse interstellar cloud (a). Over time the cloud contracts to form a dense cloud (b). Eventually the cloud collapses, forming a protostar (c). This protostar releases angular momentum through outflow of residue dust and gasses (c), forming a dense disk (d). Inside this disk particles attract each other and form planets (e). When the star eventually nears it's end, the outer layers of the star form and excrete new dust particles. These particles form an interstellar cloud (a). Credit: K.I. Öberg [2].

This report focusses on the ice layer deposition on the interstellar dust particles (see Fig. 2.3a, b) in the beginning of the lifecycle of a star. The size of these particles is approximately distributed by  $x^{-3,5}$ , hence the bulk have a size ranging from a few atoms to 0,1  $\mu\text{m}$ . If most of the oxygen is deposited on the dust grains as  $\text{H}_2\text{O}$ , as might be the case in the denser cores of the interstellar clouds, a dust particle of 0,1  $\mu\text{m}$  typically is enclosed by approximately 100 monolayers of  $\text{H}_2\text{O}$  ice.

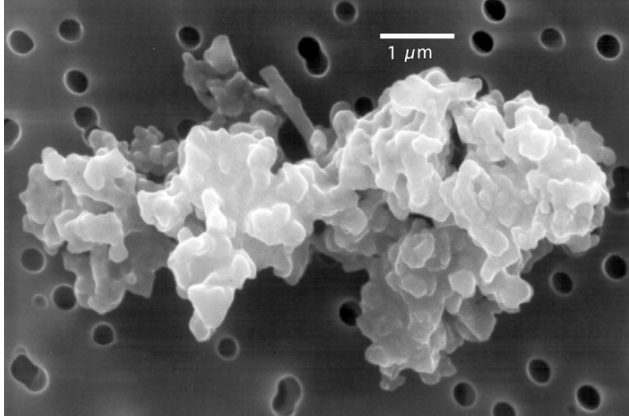


Figure 2.3: A relatively large and porous interstellar dust particle. Credit: Wikipedia - Cosmic dust [7].

Because of the high abundance of hydrogen in interstellar clouds (see Table 2.1), the forming of molecules in interstellar dust clouds happens mostly through the bombardment with hydrogen (hydrogenation). Water is formed when a deposited oxygen atom is being bombarded by hydrogen. The more complex molecules found in interstellar clouds are mostly created through hydrogenation of N, O and C atoms. So far about 180 different kind of species have been detected in interstellar space, of which most are carbon based molecules [1]. An important factor in the formation of these molecules is the porosity of the ice layers on the dust particles. Depending on the temperature during and after the deposition, the microscopic structure of the ice layer differs. Most dust particles are embedded in amorphous (unstructured) ice, however, the porosity varies. It is suspected that under influence of UV radiation or thermal warming over time the porosity decreases. Since the amount of pores increases the active surface area, the porosity acts as a catalyst and is an important factor in the efficiency of the reactions taking place on the dust particles.

Table 2.1: Relative solar elemental abundance w.r.t. hydrogen. Credit: E.F. van Dishoeck [1]

Element	Rel. Abundance w.r.t. H
H	1.00
He	0.085
N	$6.8 \cdot 10^{-4}$
O	$4.9 \cdot 10^{-4}$
C	$2.7 \cdot 10^{-4}$
Mg	$4.0 \cdot 10^{-5}$
Fe	$3.2 \cdot 10^{-5}$
Si	$3.2 \cdot 10^{-5}$
S	$1.3 \cdot 10^{-5}$
Al	$2.8 \cdot 10^{-6}$
Na	$1.7 \cdot 10^{-6}$
P	$2.6 \cdot 10^{-7}$

Table 2.2: Molecules detected in interstellar clouds. Credit: E. Gibb *et al.* [11]

Molecule	Abundance % w.r.t. $\text{H}_2\text{O}$
$\text{H}_2\text{O}$	100
$\text{CO}_2$	7 – 25
$\text{CH}_3\text{OH}$	2 – 25
$\text{H}_2\text{CO}$	3 – 7
$\text{C}_2\text{H}_6$	$\leq 0,4$
$\text{NH}_4^+$	3 – 17
CO	3 – 50
$\text{NH}_3$	$\leq 10$
$\text{CH}_4$	0,9 – 1,9
OSC	0,1
$\text{OCN}^-$	$\leq 1,9$
HCOOH	$\leq 1,7$

## 2.2 Infrared spectroscopy

Since infrared spectroscopy reveals information about the bonds between atoms, infrared measurements are commonly done by astronomers to research the molecules formed in interstellar clouds. In order to be observed, the cloud has to enclose or be in front of an infrared source. A background star is used as a source and after the infrared light passes through the cloud, only the light at wavelengths that are not absorbed by the different components of the cloud are observed at an earth based observatory. The observations are done by telescopes placed on mountains (ALMA) or in airplanes (Kuiper Airborne Observatory, SOFIA). The high altitude minimizes the absorbing and refracting effects of earth's atmosphere on the incident light. Besides earth based and airborne observatories, there also exists observatories in space (ISO, Spitzer). These space observatories experience no influence from earth's atmosphere, therefore enabling a higher resolution.

The different ice components (molecules) all have their own characteristic fingerprint; the infrared absorption spectra. This absorption behaviour is caused by changes in the vibrational motions of the atomic bindings in molecules. There are several different ways a molecule can vibrate. Generally the amount of normal modes of vibrations are given by  $3N - 6$ , in which  $N$  is the number of atoms in a molecule. For linear molecules the amount of normal modes of vibrations are given by  $3N - 5$ . In case of a  $C_2H_4O$  (formaldehyde) molecule, the amount of normal modes is  $3 \cdot 4 - 6 = 6$  (see Fig. 2.4). The molecular rotations are disregarded in this research, since molecules cannot rotate when embedded in an ice layer.

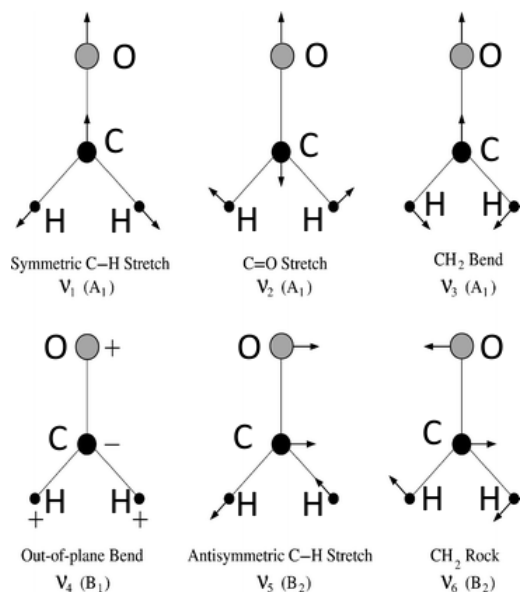


Figure 2.4: Six normal vibrational modes of formaldehyde. Credit: R.J. Bouwens *et al.* [8]

Infrared absorption arise from transitions between quantized energy levels of which the absorption  $\delta E$  corresponds to the mid-infrared energy  $h\nu$ , where  $\nu$  is the frequency and  $h$  is the Planck constant. If the molecule has a dipole moment, the radiation field will couple with it to induce transitions when the frequency of the radiation  $h\nu = \delta E$ . The vibrations of the molecular bindings can be approximated by the harmonic oscillator, which consists a mass connected by a spring to an immovable object. The angular frequency of oscillation  $\omega$  is given by:

$$\omega = \sqrt{\frac{k}{m}} \quad (2.1)$$

in which  $k$  is the spring constant, or bonding constant and  $m$  the mass of the object. The angular frequency  $\omega$  equals  $2\pi\nu$ , in which  $\nu$  is the frequency. This is inserted into Eq. 2.1 and solved for

frequency  $\nu$ . Furthermore, eq. 2.1 assumes that the system consists of only one mass, attached to an immovable object. In practice the system has two moving masses, namely the masses of the two bonded atoms. The reduced mass  $\mu$  of two bonded atoms equals  $\frac{m_1 m_2}{m_1 + m_2}$ , in which  $m_1$  and  $m_2$  are the atomic masses of the two bonded atoms:

$$\nu = \frac{1}{2\pi} \sqrt{\frac{k}{\mu}} \quad (2.2)$$

As a result of the Schrödinger wave equation, the energy of the vibrations is quantized:

$$E_n = h(n + \frac{1}{2})\nu \quad (2.3)$$

where  $n$  is the quantum number (0, 1, 2, 3, ...) and  $h$  is the Planck constant <sup>1</sup>. A more accurate approximation is given by the Morse potential, which takes into account the dissociation energy required to break the bond between the two atoms (see fig. 2.5).

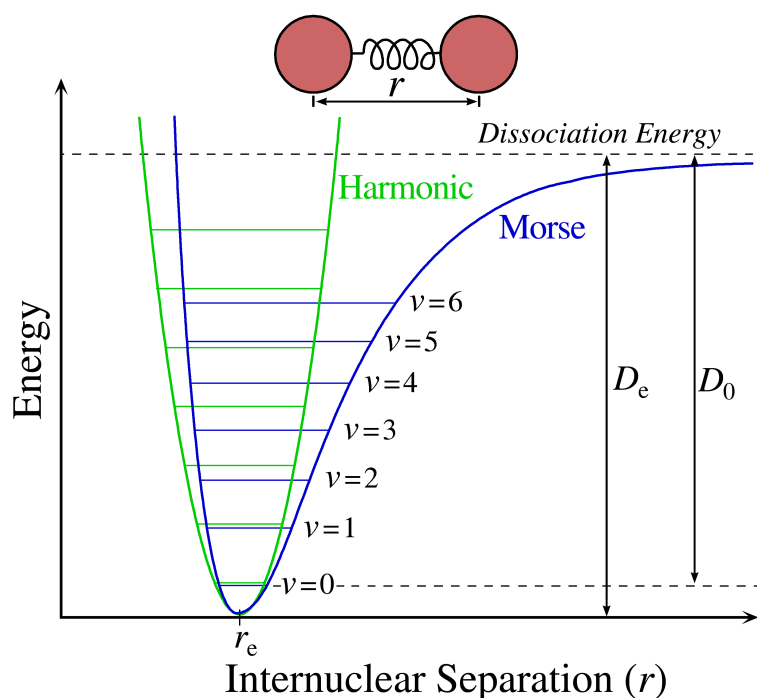


Figure 2.5: Energy of a vibrational state as a function of the internuclear separation. Note the dissociation energy  $D_e$  and the true energy required to break the bond  $D_0$ , which is smaller due to the zero point energy ( $v=0$ ) at the lowest energy level. Credit: Wikipedia - Morse Potential [10].

As atomic masses and force constants differ, each type of bonding and associated atoms have a distinct wavelengths of radiating with which they interact. When a broadband source is used to illuminate the researched substance, a spectrum with absorbance peaks can be constructed. This is done for different molecules suspected to be present in interstellar clouds. In the the Sackler Lab at the Leiden University the spectra are acquired from experiments in which the harsh interstellar environment is simulated. With the help of these spectra, astronomers can quantify what absorption peaks indicate the presence of what

<sup>1</sup>The Planck constant  $h$  describes the relationship between energy and frequency, and is equal to  $6,626 \cdot 10^{-34} \text{J} \cdot \text{s}$  or  $4,136 \cdot 10^{-15} \text{eV} \cdot \text{s}$

molecules in the clouds (see Fig. 2.6). This helps astronomers better understand the chemical processes taking place on the dust particles.

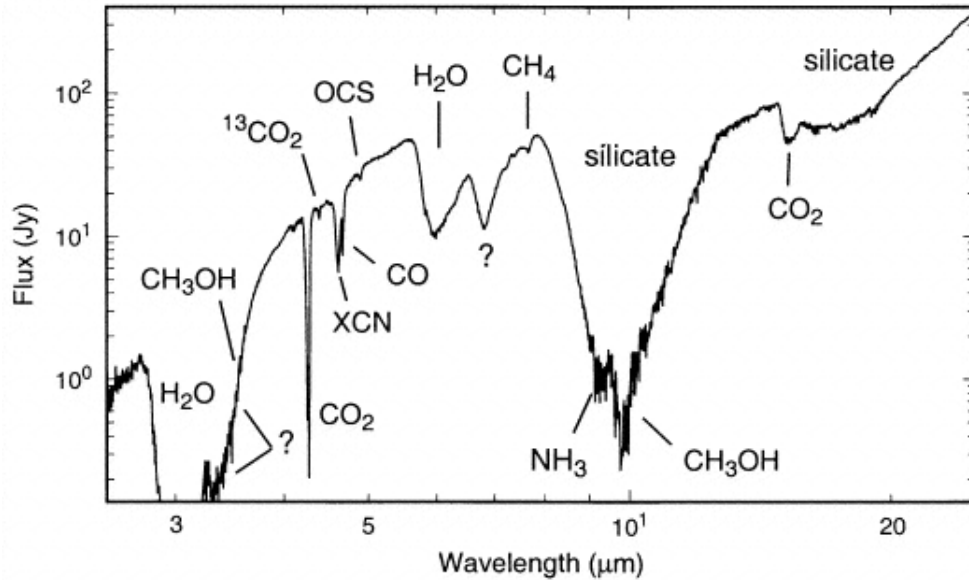


Figure 2.6: The infrared absorption spectrum of interstellar dust surrounding the star W33A. Note the question marks at the unknown peaks. Credit: E. Gibb *et al.* [11]

## 2.3 Deposition rate

Optical laser interference and infrared spectroscopy cannot be performed simultaneously because of geometrical restrictions in the HV-setup. Laser optical interference allows ice thickness determination with a good accuracy. For the wavelength dependent optical constants in the mid-infrared it is essential to know the ice layer thickness. The deposition rate is controlled by the needle valve between the sample bulb and vacuum chamber. Since this valve only displays an arbitrary unit, the ice layer thickness is measured by optical laser interferometry. Optical laser interferometry is based on the analysis of the interference fringes. The fringes are a result of interference between reflected light off the vacuum/ice and off the ice/substrate interface.

In order to calculate the reflected light intensity as a result of the interference, the refractive indices of the vacuum  $n_1$ , the ice  $n_2$  and the substrate  $n_3$  have to be known. Snell's law describes the relationship between the angle of incidence  $\theta_1$  and refraction  $\theta_2$ , when light travels through the interface of two media with different refractive indices:

$$n_1 \sin \theta_1 = n_2 \sin \theta_2 \quad (2.4)$$

Note that the used silicon substrate is opaque for the He-Ne laser light, so all the light is reflected at the silicon surface. The refractive index of the vacuum  $n_1$  and silicon substrate  $n_3$  are considered constant in this report. The refractive indexes of the deposited ices are extracted from literature or measured.

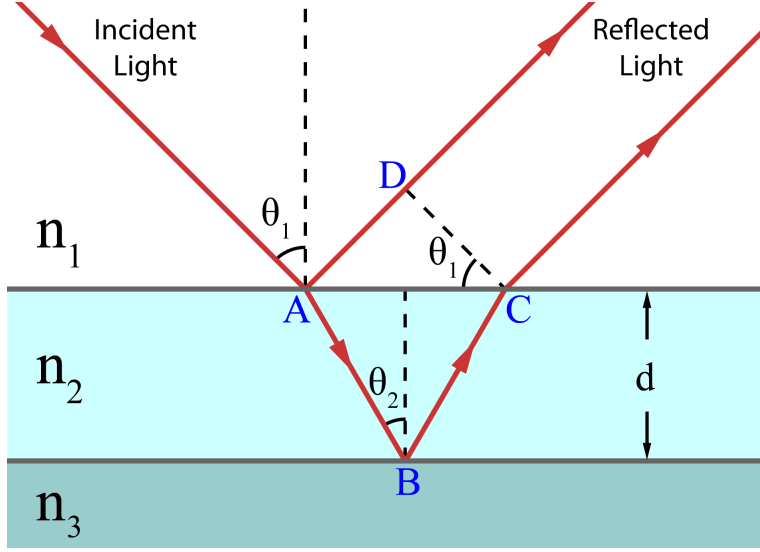


Figure 2.7: Schematic of optical interferometry inside a three layer structure. Credit: Wikipedia - Thin-film interference [13]

Since light is reflected at point A and point B (see fig. 2.7), these beams will interfere. The interference (constructive or destructive) depends on the phase difference between the two beams. This depends on the thickness and the refractive index of the ice  $n_2$  and the angle of the incident light  $\theta_1$ . It is important to note that the refractive index  $n_2$  is wavelength dependent. However, by using a HeNe laser, only one value for  $n_2$  can be used. The optical path difference (OPD) for reflected beams is given by:

$$OPD = n_2(l_{AB} + l_{BC}) - n_1(l_{AD}) \quad (2.5)$$

in which  $l_{xx}$  is the path length between two points in fig. 2.7.  $l_{AB}$  and  $l_{BC}$  can be written as:

$$l_{AB} = l_{BC} = \frac{d}{\cos(\theta_2)} \quad (2.6)$$

the term  $l_{AD}$  can be written as:

$$l_{AD} = 2d \tan(\theta_2) \sin(\theta_1) \quad (2.7)$$

inserting eq. 2.6 and eq. 2.7 into eq. 2.5 gives:

$$OPD = n_2 \frac{2d}{\cos(\theta_2)} - n_1 2d \tan(\theta_2) \sin(\theta_1) \quad (2.8)$$

using eq. 2.4, this forms into:

$$OPD = n_2 \frac{2d}{\cos(\theta_2)} - n_2 2d \tan(\theta_2) \cos(\theta_2) \quad (2.9)$$

which can be written as:

$$OPD = 2dn_2 \frac{1 - \sin^2(\theta_2)}{\cos(\theta_2)} \quad (2.10)$$

this is simplified to:

$$OPD = 2dn_2 \cos(\theta_2) \quad (2.11)$$

the interference is constructive when OPD equals a multiple of the wavelength:

$$m\lambda = 2dn_2 \cos(\theta_2) \quad (2.12)$$

in which  $m$  is an integer (1, 2, 3...) and  $\lambda$  the wavelength of the used light. During deposition, the thickness  $d$  increases linearly. This increases the value for  $m$ , which means that the interference moves from constructive to destructive (see fig. 2.8). Since the interference peaks occur at a multiple of  $\frac{1}{2}$ , the associated ice layer thickness can be calculated through the use of eq. 2.12. When the position of the peaks is determined, the deposition rate can be determined through the application of linear regression. This results in a function describing the deposition rate as a function of time (see section 4.3.1 & appendix B.1). The deposition coefficient  $\gamma$  relates to the ice layer thickness  $d$  by:

$$d(t) = \gamma t + d(0) \quad (2.13)$$

in which  $d(t)$  is the layer thickness as a function of time  $t$ . The term  $d(0)$  described the initial ice layer thickness, caused by residual gasses depositing during the cooling of the substrate. It is important to note that from this point on, the ice layer thicknesses and related formula are given in nm.

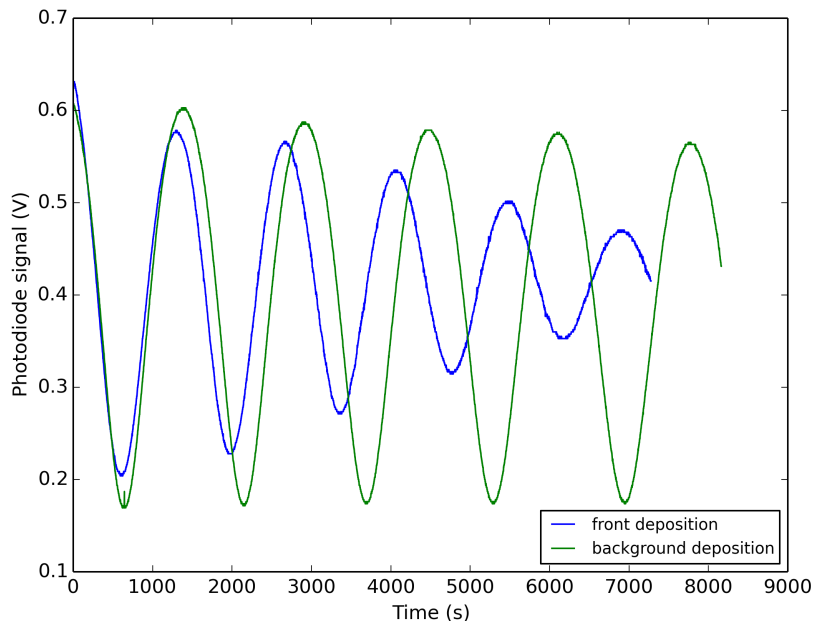


Figure 2.8: A typical interference signal, as a function of a growing of a thickness increase over time. Note the damping effect on the amplitude of the peaks for the front deposition. This is caused by the over time roughening of the ice surface.

## 2.4 Optical constants

An electromagnetic wave consists of a varying electric and magnetic field. When this wave travels through a medium, the electric and magnetic component can interact with the medium. The electric field can change the dipole moment of the molecules embedded in the medium, which then decreases the velocity of the wave. The velocity  $v$  of an electromagnetic wave in a medium is given by:

$$v = \frac{1}{\epsilon_r \epsilon_0 \mu_0} \quad (2.14)$$

in which  $\epsilon_r$  is the relative permittivity of the medium,  $\epsilon_0$  the absolute permittivity and  $\mu_0$  the absolute permeability. For free space, the relative permittivity  $\epsilon_r$  equals 1. It is important to note that the value of  $\epsilon_r$  is frequency dependent. [14] Since the refractive index  $n$  is a measure of the ratio of the speed of light  $c$  in free space and a medium,  $n$  is given by:

$$n = \frac{c}{v} = \sqrt{\epsilon_r} \quad (2.15)$$

As seen in eq. 2.4, the refractive index  $n$  determines the amount of refracted for incident light travelling through the surface of different media. Taking absorption into account, the complex refractive index is defined by:

$$N = n - ik \quad (2.16)$$

in which the imaginary variable  $k$  indicates the absorption of the electromagnetic wave through a medium [15]. In an international collaboration with the dr. B. Mate, the wavelength dependent values of  $n$  and  $k$  of the measured spectra are determined through the use of the Kramer-Kronig equation. This equation calculates relationship between the real and imaginary part of a complex function, given that the imaginary part is in the upper half plane. The wavelength dependent optical constants of  $n$  and  $k$  are calculated for a non-porous single component ice ( $\text{CH}_4$  and  $\text{H}_2\text{O}$ ). These values can be used to predict the effective optical constants for a porous three component ice mixture, given that there is no interaction between the components (such as the forming of hydrogen bonds). The prediction is done by the use of theoretical modelling, by which the macroscopic properties of composite materials are described. To do so, the extended Bruggemans Effective Medium Approximation is used:

$$f_A \frac{\epsilon_A - \epsilon_{\text{eff}}}{\epsilon_A + 2\epsilon_{\text{eff}}} + f_B \frac{\epsilon_B - \epsilon_{\text{eff}}}{\epsilon_B + 2\epsilon_{\text{eff}}} + f_C \frac{\epsilon_C - \epsilon_{\text{eff}}}{\epsilon_C + 2\epsilon_{\text{eff}}} = 0 \quad (2.17)$$

in which  $f_X$  is the volume fraction of component X and  $\epsilon_X$  the temperature dependent effective dielectric constant. The term  $\epsilon_{\text{eff}}$  relates to the relative dielectric constant of the three component system. The component A is pores, B is  $\text{H}_2\text{O}$  and C is  $\text{CH}_4$ . The dielectric constants  $\epsilon_X$  in eq. 2.17 are then replaced by  $n^2$ , given that  $\epsilon_X = n^2$ . However, taking into account the absorption of the medium, eq. 2.16 is used. Assuming the relative dielectric constant of the pores  $\epsilon_A$  is 1, eq. 2.17 becomes:

$$f_A \frac{1 - N_{\text{eff}}^2}{1 + 2N_{\text{eff}}^2} + f_B \frac{N_B^2 - N_{\text{eff}}^2}{N_B^2 + 2N_{\text{eff}}^2} + f_C \frac{N_C^2 - N_{\text{eff}}^2}{N_C^2 + 2N_{\text{eff}}^2} = 0 \quad (2.18)$$

in which  $N$  is the complex refractive index (see eq. 2.16). The values for  $n$  and  $k$  of  $N_{\text{eff}}$  are determined for a range of porosity fractions  $f_A$ , through the use of a written Python program (see appendix B.3). The Python program first calculates the complex refractive indices  $N_B$  and  $N_C$ . For a range of volume fractions of the pores  $f_A$ , the effective complex refractive index of the mixture is calculated. This yields three solutions, with each a real and imaginary part. However, two of these solutions have a negative real value, hence they are discarded. Following, the program solves for  $n_{\text{eff}}$  and  $k_{\text{eff}}$ . Since  $N^2 = n^2 - k^2 - i2nk$ , the values of  $n_{\text{eff}}$  and  $k_{\text{eff}}$  can be calculated by solving the complex refractive index for its real and imaginary part, which results in a nonlinear system with two unknowns:

$$N_{\text{real}} = n^2 - k^2 \quad (2.19)$$

$$N_i = -i2nk \quad (2.20)$$

# Chapter 3

## HV-setup

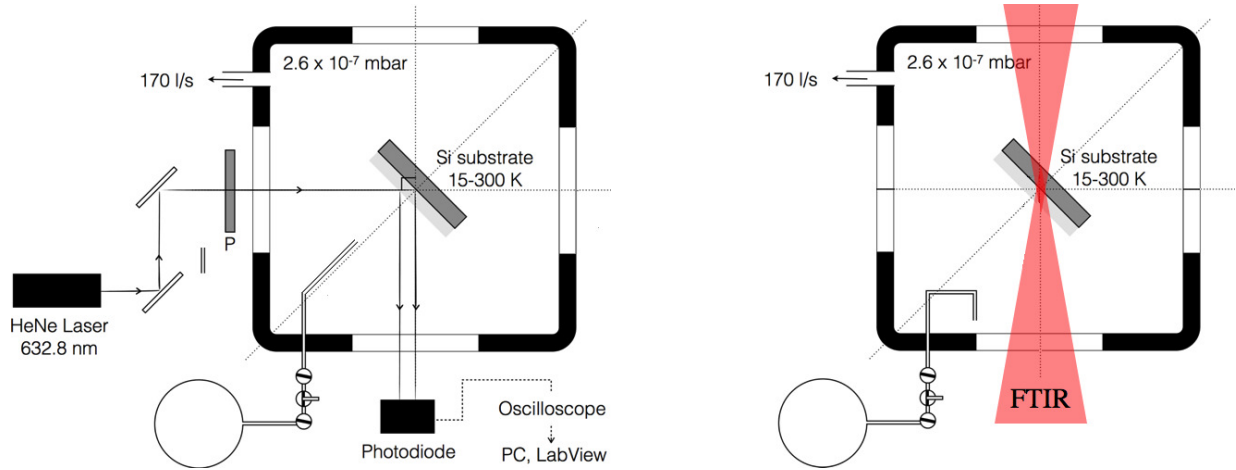
The HV (high vacuum) setup is used in two configurations, namely for optical interferometry and infrared spectroscopy (see Fig. 3.1). Besides the components used for these configurations, the setup consists of a vacuum and cryogenic system.

### 3.1 Vacuum system

The vacuum system consists of a vacuum chamber, in which a silicon substrate is placed at a 45° angle with respect to the incident laser beam. The silicon substrate is transparent for mid infrared light, but is however opaque for the used HeNe laser light. The vacuum chamber is pumped by a TPH170 Pfeiffer/Balzers turbo pump, backed by an Edward E2M8 rotary vane dual stage pump. This enables the chamber to reach a pressure of  $2.0 \cdot 10^{-7}$  Torr<sup>1</sup>. The pressure is measured by a Bayert-Alphert ionization gauge. To cool the substrate to cryogenic temperatures, a closed cycle helium cryostat is used. The cryostat cools the substrate to 17 K. The substrate is placed in a gold plated copper holder to allow for efficient cooling. By using a copper resistive heating filament, the substrate can be heated to higher temperatures, with an accuracy of 0.1 K. The vacuum chamber has four windows, to allow for the optical interferometry and infrared spectroscopy to be performed. Two of the windows are made of potassium bromide (KBr). This is required for the infrared spectroscopy, as they are transparent for infrared light. The sample gas is let into the vacuum chamber through a needle valve, which controls the deposition rate. Different deposition modes are available through the use of the two gas inlets onto the vacuum chamber, depending on the wanted structure of the ice. When a compact (non-porous) amorphous ice is wanted, front deposition is used (see Fig. 3.1a). However, this deposition method grows an ice layer with a pyramidal (non-flat) shape. In order to deposit a flat ice layer, background deposition is used (see Fig. 3.1b). Since instead of introducing the molecules in the direction of the cold substrate (front deposition), this mode fills the entire vacuum chamber with molecules. As a result the molecules that do deposit onto the substrate, deposit at random angles. This increases the porosity, but also forms a homogeneous ice layer.

---

<sup>1</sup>1 Torr = 1.333224 mbar



(a) The optical interferometry configuration in front-deposition mode. Note the sample inlet aimed at the substrate.

(b) The infrared spectroscopy configuration in back-ground deposition mode. Note the sample inlet aimed away from the substrate.

Figure 3.1: Schematics of the HV-setup in two different configurations. The circles in the lower-left corner represent the glass sample bulb. Note the use of the lower window for both optical interferometry and infrared spectroscopy. Credit: K. Isokoski *et al.* [12].

## 3.2 Optical interferometry system

For optical interferometry, an intensity stabilized Thorlabs HRS015 HeNe laser is used (see Fig. 3.1a), which emits a 1.2 mW beam of light at a wavelength of 632.8 nm. Through the use of a linear polariser the laser light is polarized in the direction perpendicular with respect to the plane of incidence on the substrate (s-polarized). The laser light then is partially reflected off the surface, and partially by the substrate. These light beams interfere with each other. By measuring the intensity of the reflected light at a constant angle, the deposition rate can be determined (see chapter 2.3). The intensity of the light is being measured by a Thorlabs PDA36A photodiode. An oscilloscope is used to transform the signal from analogue to digital. A computer with a LabVIEW program is used to record this signal and the temperature, as a function of time.

### 3.3 Infrared spectroscopy system

To measure the infrared spectrum of the ice layer, the photodiode is removed from the setup. This allows for the infrared light to pass through the vacuum chamber and substrate. Inside the infrared spectrometer is an infrared source, which emits broadband infrared light at a range of  $4000 - 400\text{cm}^{-1}$ <sup>2</sup>. Before the ice layer deposition, a reference measurement is done. The acquired spectrum is called the *background spectrum*, which functions as a reference for post-deposition measurements. The ratio of wavelength dependent intensities of the background and post-deposition spectra are used to calculate the absorbance  $A$ , through the use of the law of Lambert-Beer:

$$A = \log \frac{I_0}{I} \quad (3.1)$$

where  $I_0$  is the intensity of the background light and  $I$  of the post-deposition spectrum. In this report, only ice layers are grown with absorbance up to  $A \approx 0,9$ . This ensures the linear response of the law of Lambert-Beer. The absorbance at each wavenumber differs, depending on the used sample. The spectra are measured by a Varian 670 FT-IR spectrometer. Each spectrum is averaged over 512 times (11 minutes acquisition time per spectrum) and has a resolution  $2\text{cm}^{-1}$  resolution.

---

<sup>2</sup>The wavenumber is a unit of cycles per distance ( $\text{cm}^{-1}$ ). It is used as an alternative for wavelengths, since it proportionally relates with frequency and photon energy.

# Chapter 4

## Results

Considering the limitations of the current setup, the deposition rate is determined for a certain setting of the needle valve (see Fig. 3.1). From the deposition rate, an ice layer thickness is calculated for each acquired spectrum. This is needed for the optical constants to be calculated. From these constants the effective optical constants of an ice mixture of H<sub>2</sub>O and CH<sub>4</sub> are predicted. It is important to note that two different approaches for measuring the spectra have been considered. One method consists of measuring multiple spectra, for different ice layer thicknesses, during one experiment (day). However, it was found that the uncertainty in one of the methods increased greatly (see annex C). Because of this it was decided to divide the spectra measurements over multiple days, so one spectrum a day is measured. The ice layers are all deposited and measured at 30 K, except for the pure H<sub>2</sub>O ice, which was deposited at 120 K and measured at 30 K.

### 4.1 Compact & pure CH<sub>4</sub>

Previous measurements have been done with H<sub>2</sub>O to determine the correct setup settings for a deposition rate of  $\simeq 0.2\text{nm} \cdot \text{s}^{-1}$ , in order to acquire a good resolution. Since the porosity depends on a number of factors, including the deposition rate, a similar deposition rate is wanted. This ensures a constant porosity for both H<sub>2</sub>O and CH<sub>4</sub>. After experimentally determining the correct settings for a similar deposition rate for CH<sub>4</sub>, the experiment is repeated four times so the uncertainty can be calculated. Using the written Python program (see annex B.2, the peak positions are determined with related ice layer thicknesses.

#### 4.1.1 Deposition rate

To determine the deposition rate, the calculated ice layer thicknesses (see Eq. 2.13) are plotted as a function of time. By applying linear regression, a function is found which describes the slope and offset of the line. This function directly describes the deposition rate. From the written Python program (see annex B.2), it was found that the deviation from the mean increases when all datapoints (calculated thicknesses at the peaks) are combined into one dataset. From this can be concluded that the uncertainty of the linear equation (describing the deposition rate) is mostly determined by a day to day variation in deposition rate, and not the method of determining the peak positions. Using a written Python program (see annex B.2), all datapoints from different experiments are combined to form one dataset of 40 ice layer thicknesses with associated time values, from which a standard deviation for the slope  $\sigma_a$  and offset  $\sigma_b$  is calculated (see Fig. 4.1).

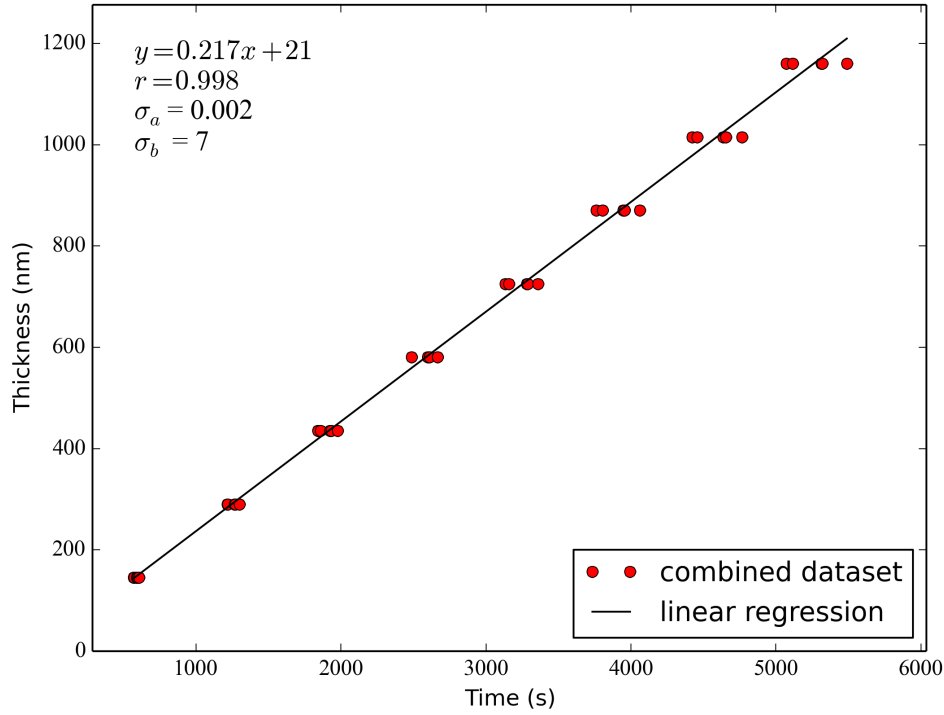


Figure 4.1: The ice layer thickness as a function of time for the combined dataset of five experiments. Note the linear relationship  $y(x)$ , the correlation coefficient  $r$ , and the standard deviation in the slope  $\sigma_a$  and offset  $\sigma_b$ .

By inserting the found slope, offset and two times the standard deviations ( $2 \cdot \sigma$ ) (see Fig. 4.1) in eq. 2.13, a formula is created to describe the deposition rate range in which 95.45% of the experiments will fall:

$$d_{\text{CH}_4}(t) = (0.217 \pm 0.004) \cdot t + (21 \pm 14) \quad (4.1)$$

#### 4.1.2 Measurements spectra & optical constants

The absorption spectrum of  $\text{CH}_4$  shows the two absorption peaks in the  $4000 - 400\text{cm}^{-1}$  region. Besides these two narrow peaks, the absorbance is negligible. To display the spectra in more detail, the peaks are magnified by removing sections of the spectra where the absorbance is negligible (see Fig. 4.2). The spectra are measured for five different ice layer thicknesses, to acquire a better accuracy in the optical constants.

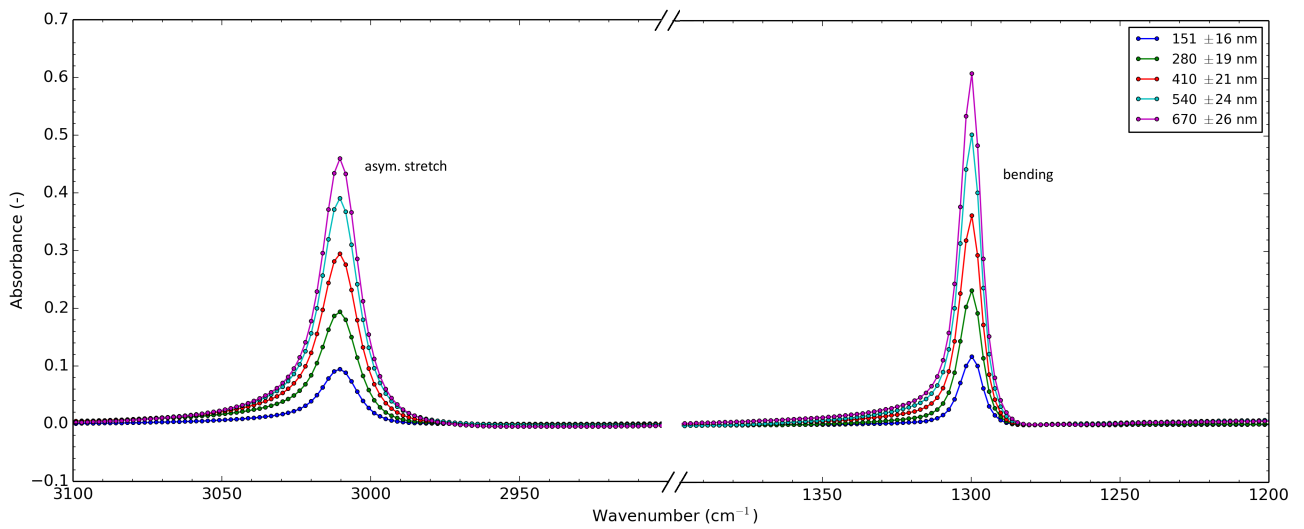


Figure 4.2: The two absorption peaks of  $\text{CH}_4$  in the  $4000\text{-}400\text{ cm}^{-1}$  range.

Through the use of the Kramer-Kronig equation the optical constants  $n$  and  $k$  for the absorption spectra of pure and compact (non-porous)  $\text{CH}_4$  are determined.

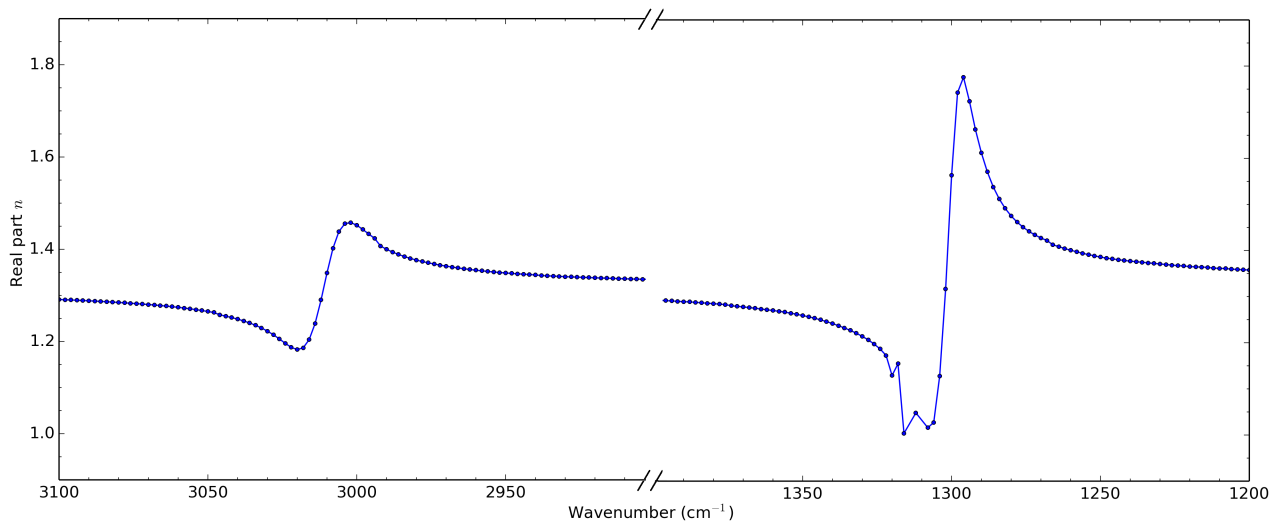


Figure 4.3: The real part  $n$  of the complex refractive index of  $\text{CH}_4$ , for the two absorption peaks in the  $4000\text{-}400\text{ cm}^{-1}$  range.

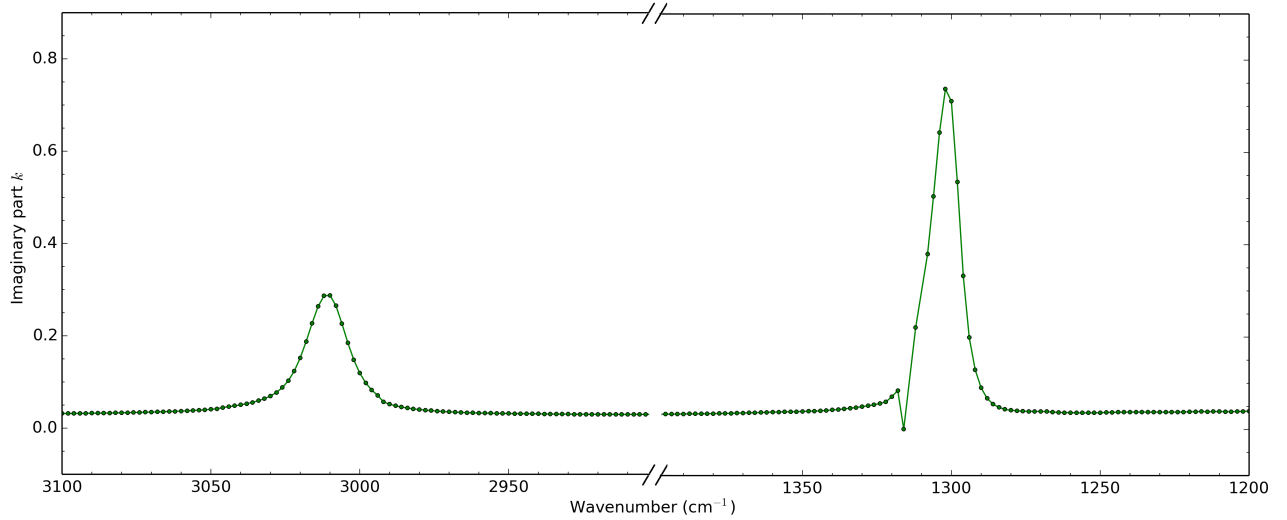


Figure 4.4: The imaginary part  $k$  of the complex refractive index of  $\text{CH}_4$ , for the two absorption peaks in the  $4000\text{-}400\text{ cm}^{-1}$  range.

## 4.2 Compact & pure $\text{H}_2\text{O}$

In previously done experiments [16], the deposition rate for water is determined by the use of the method earlier described for  $\text{CH}_4$  (see chapter 2.3 & 4.1.1). The deposition rate which describes 95.45% the experiments' deposition rate for  $\text{H}_2\text{O}$  is given by:

$$d_{\text{H}_2\text{O}}(t) = (0.191 \pm 0.004) \cdot t + (10 \pm 16) \quad (4.2)$$

### 4.2.1 Measurements spectra & optical constants

The absorption spectrum of  $\text{H}_2\text{O}$  also shows the two large absorption peaks in the  $4000 - 400\text{cm}^{-1}$  region. Due to baseline corrections and very weak absorption, it was decided to not display the relatively small absorption peaks at in the  $2900 - 1700\text{cm}^{-1}$  range. To display the spectra in more detail, the  $\text{H}_2\text{O}$  peaks too are magnified by removing sections of the spectra where the absorbance is negligible (see Fig. 4.6). The spectra are measured for five different ice layer thicknesses, to acquire a better accuracy in the optical constants.

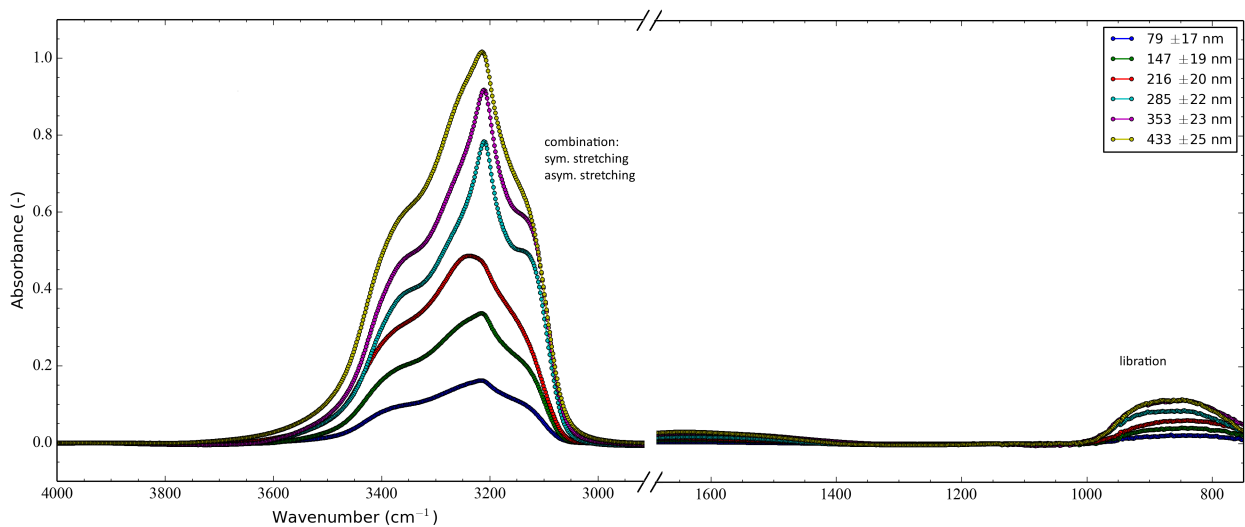


Figure 4.5: The two main absorption peaks of  $\text{H}_2\text{O}$  in the  $4000 - 400\text{cm}^{-1}$  range.

Through the use of the Kramer-Kronig equation the optical constants  $n$  and  $k$  for the absorption spectra of pure and compact (non-porous)  $\text{H}_2\text{O}$  are determined.

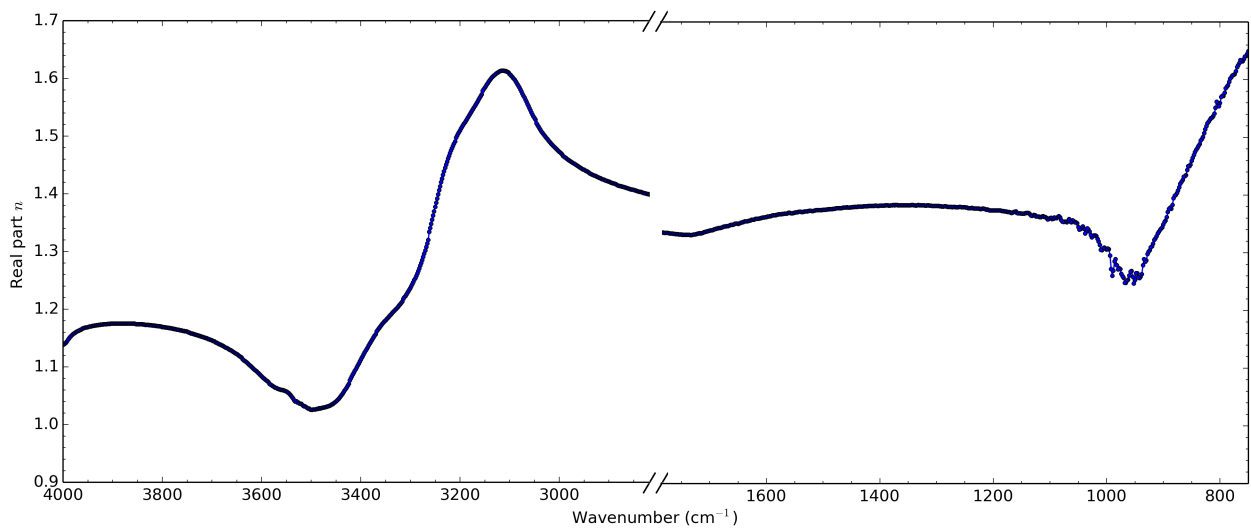


Figure 4.6: The real part  $n$  of the complex refractive index of  $\text{H}_2\text{O}$  in the  $4000\text{-}400\text{ cm}^{-1}$  range.

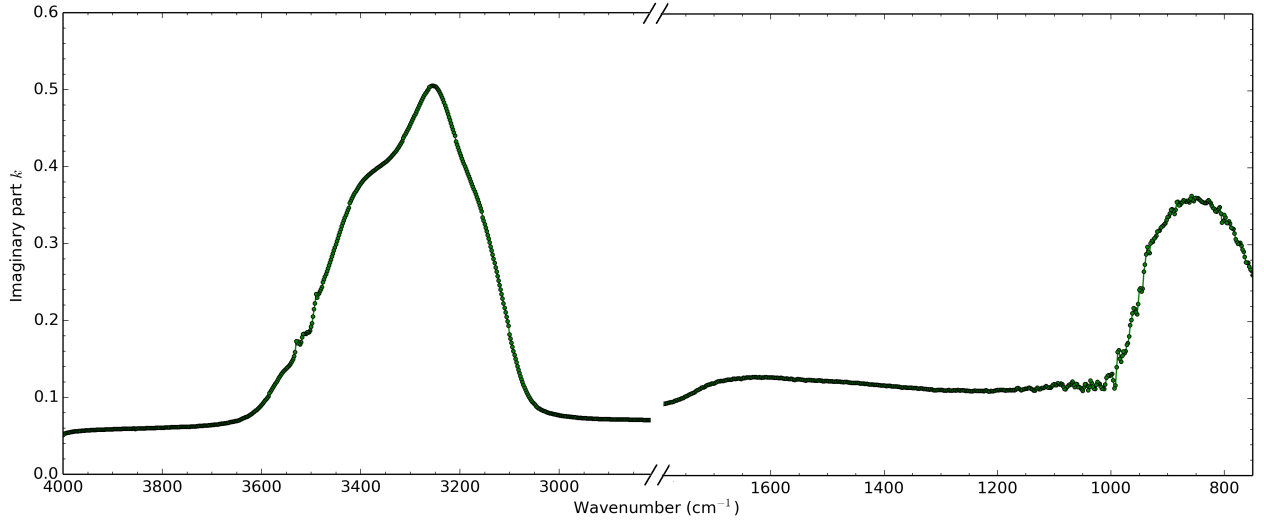


Figure 4.7: The imaginary part of the complex refractive index  $k$  of  $\text{H}_2\text{O}$  in the  $4000\text{-}400\text{ cm}^{-1}$  range.

It is important to note that contrary to  $\text{CH}_4$ , the absorbance of  $\text{H}_2\text{O}$  is never truly 0. This complicates the calculations of the optical constants by the use of the Kramer-Kronig equation, which results in less accurate values.

### 4.3 Porous mixture $\text{H}_2\text{O}:\text{CH}_4$ (2:1)

By inserting the  $n$  and  $k$  values of pure and compact (non-porous)  $\text{H}_2\text{O}$  and  $\text{CH}_4$  ice into the written Python program (see annex B.3), the effective optical constants can be calculated (see 2.4).

#### 4.3.1 Deposition rate

The deposition rate for a mixture can not be calculated with the method previously described (see chapter 2.3 & chapter 4.1.1), because the refractive index  $n$  of the mixture is unknown. By using the method described by Bossa *et al.*, the refractive index and associated deposition rate is calculated. [16] The experiment for determining the deposition rate is repeated for a total of three times, due to time constraints. Nonetheless, the uncertainty is determined by calculating the standard deviation of the slope  $\sigma_a$  and offset  $\sigma_b$ . By inserting  $2\sigma_a = 0.006$  and  $2\sigma_b = 7$  into Eq. 2.13, a formula is created to describe the deposition rate range in which 95.45% of the experiments will fall:

$$d_{\text{mix}}(t) = (0.190 \pm 0.006) \cdot t + (26 \pm 7) \quad (4.3)$$

#### 4.3.2 Measurements spectra & optical constants

As done before, the spectra of the  $\text{H}_2\text{O}:\text{CH}_4$  (2:1) mixture are scaled. This again increases the detail at which the absorption peaks

The absorption spectrum of  $\text{H}_2\text{O}$  also shows the two large absorption peaks in the  $4000 - 400\text{cm}^{-1}$  region. Due to baseline corrections and very weak absorption, it was decided to not display the relatively small absorption peaks at in the  $2900 - 1700\text{cm}^{-1}$  range. To display the spectra in more detail, the  $\text{H}_2\text{O}$  peaks too are magnified by removing sections of the spectra where the absorbance is negligible (see Fig. 4.6).

The spectra are measured for five different ice layer thicknesses, to acquire a better accuracy in the optical constants.

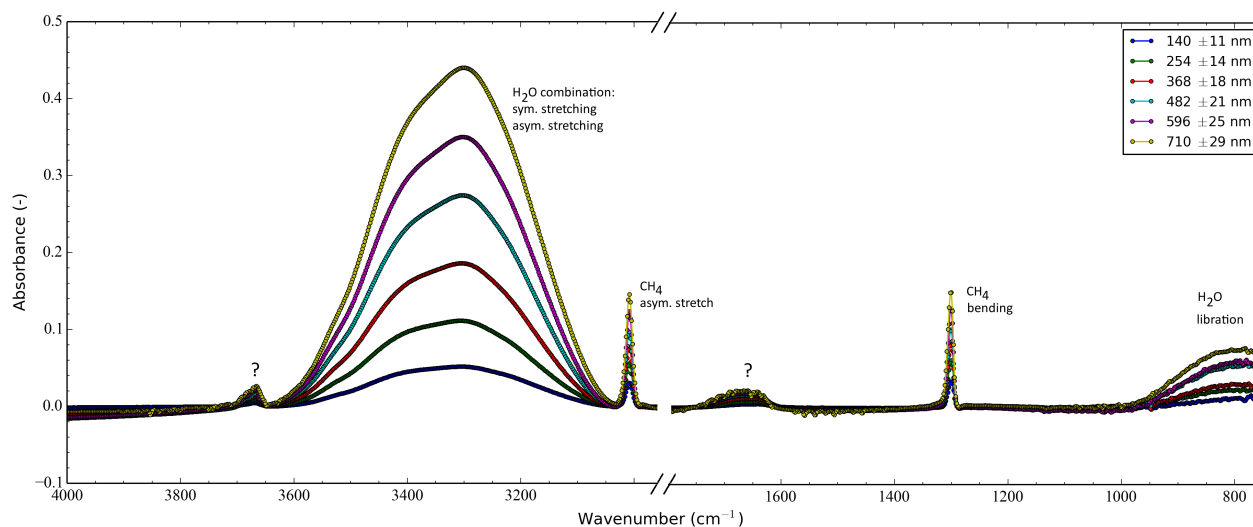


Figure 4.8: The absorption spectrum of a  $\text{H}_2\text{O}:\text{CH}_4(2:1)$  mixture. Note the question marks at the unknown peaks.

The spectra of the mixture show 'new' unknown peaks, marked by a question mark. These peaks were previously not seen in the spectra of pure and compact  $\text{H}_2\text{O}$  and  $\text{CH}_4$ . Since  $\text{CH}_4$  is a polar and  $\text{H}_2\text{O}$  a nonpolar, they are not interacting.<sup>1</sup> From this can be concluded that the new peaks are likely caused by the induced porosity. The next step is to calculate the effective optical constants for the mixture, by using the  $n$  and  $k$  values for  $\text{H}_2\text{O}$  and  $\text{CH}_4$  and through the use of the written Python program (see annex B.3).

<sup>1</sup>The polarity describes whether or not a molecule has a symmetric electric charge distribution. The molecule  $\text{H}_2\text{O}$  is an asymmetric molecule. The molecule  $\text{CH}_4$  however, is symmetric. This means that no hydrogen bonds can be formed between  $\text{H}_2\text{O}$  and  $\text{CH}_4$ , hence they do not interact.

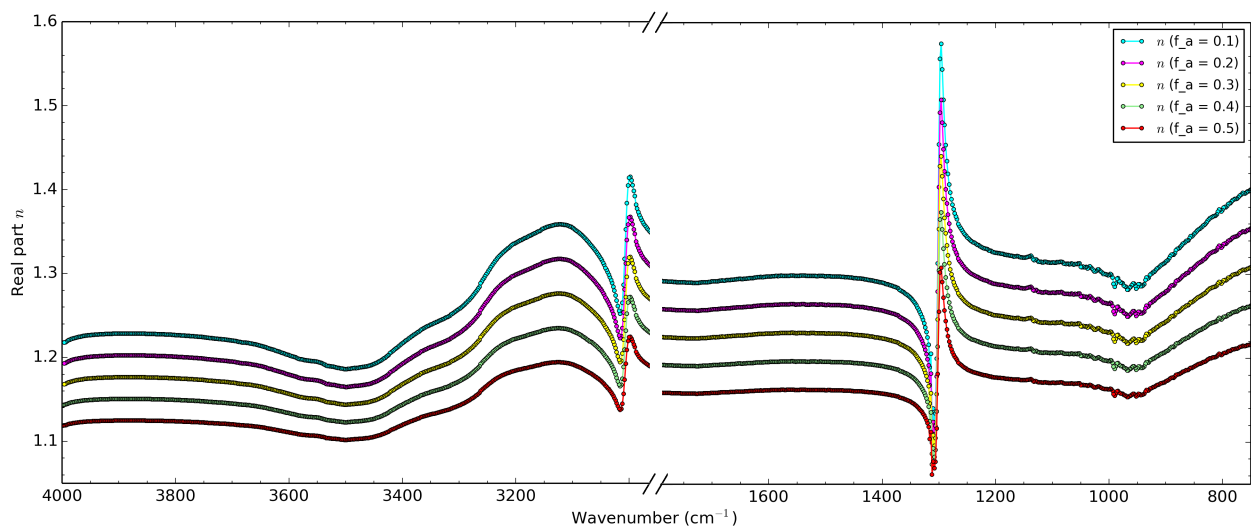


Figure 4.9: The calculated real part of the complex refractive index  $n$  of a  $\text{H}_2\text{O}:\text{CH}_4$  (2:1) mixture with different porosity volume fractions ( $f_a$ ), in the  $4000\text{-}400\text{ cm}^{-1}$  range.

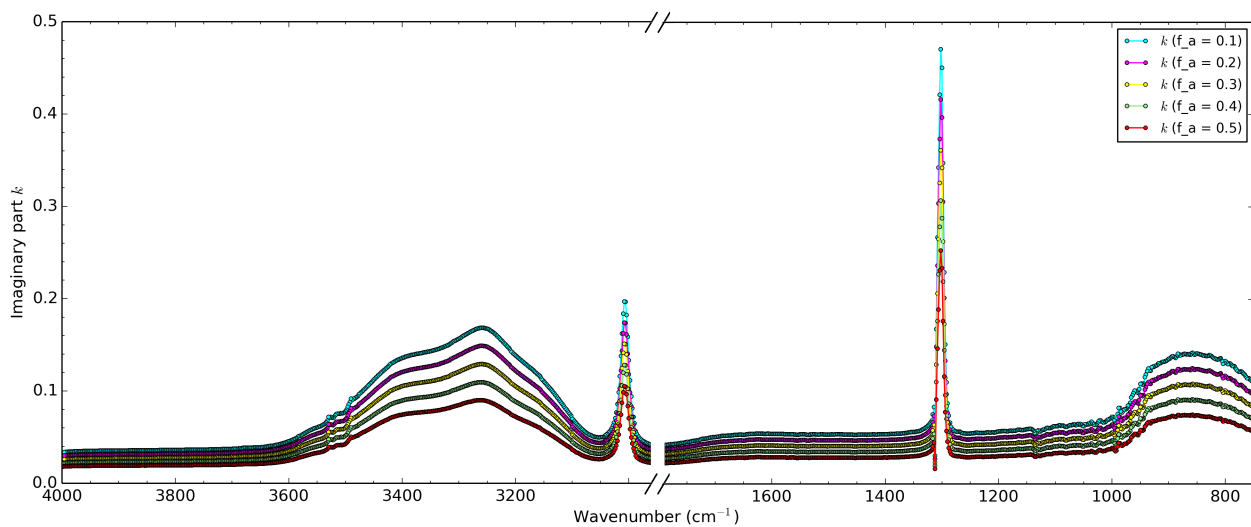


Figure 4.10: The calculated imaginary part of the complex refractive index  $k$  of a  $\text{H}_2\text{O}:\text{CH}_4$  (2:1) mixture with different porosity volume fractions ( $f_a$ ) in the  $4000\text{-}400\text{ cm}^{-1}$  range.

## Chapter 5

# Conclusion

Though the current setup complicates the measurements and increases the uncertainties, a useful method for measuring ice layer thicknesses, spectra and predicting the effective optical constants  $n$  and  $k$  of a mixture are found. The uncertainties for the ice layer thicknesses is determined. However, what the implication of the uncertainties in the ice layer thickness is on the optical constants has yet to be determined. The written Python program for calculating the effective optical constants can be extended for analysis of a mixture with unknown volume fractions, for both the pores and molecules. By predicting a spectrum from the optical constants of the individual components, the validity and accuracy of the model can be determined. It is hoped for that the 'new' peaks in Fig. 4.8 are a good measure of the porosity of the ice, and that the written Python program for calculating the effective optical constants can predict these peaks, based only on the optical constants of the individual components. Besides concentrating on 'new' peaks, different methods, such as surface calculations of the known absorption peaks can be applied. The aim is to further develop this model, so that not only spectra with different components and volume fractions can be predicted, but also unknown spectra analysed. This will be a powerful tool for astronomers.

# Bibliography

- [1] E.F. van Dishoeck. *Astrochemistry of dust, ice and gas: introduction and overview*. Faraday Discuss., 2014, 168, 9-47
- [2] K.I. Öberg, (2009). *Complex processes in simple ices. Laboratory and observational studies of gas-grain interactions during star formation*. PhD thesis, Sackler laboratory, Leiden Observatory, Leiden University.
- [3] Earthsky.org Visited: 10-12-2014.  
<http://earthsky.org/space/rosettas-comet-fuels-debate-on-origin-of-earths-oceans>
- [4] ESA/NASA Hubble database. Visited: 03-11-2014.  
<http://sci.esa.int/hubble/46921-spectacular-landscape-in-the-carina-nebula/>
- [5] EarthSky: "Did comets bring water to Earth?" Visited: 27-11-2014.  
<http://earthsky.org/space/did-comets-bring-water-to-earth>
- [6] Space.com: "Life's Building Blocks 'Abundant In Space'". Visited: 17-10-2014.  
<http://www.space.com/1686-life-building-blocks-abundant-space.html>
- [7] Wikipedia: "Cosmic dust". Visited: 04-11-2014. [http://en.wikipedia.org/wiki/Cosmic\\_dust](http://en.wikipedia.org/wiki/Cosmic_dust)
- [8] R. J. Bouwens *et al.* *Pure vibrational spectroscopy of S<sub>0</sub> formaldehyde by dispersed fluorescence*. J. Chem. Phys., 1996, 104, 460
- [9] P.F. Bernath, (2005). *Spectra of Atoms and Molecules* (pp. 208-226). Oxford University Press, ISBN: 978-0-19-517759-6
- [10] Wikipedia: Morse Potential. Visited: 28-11-2014. [http://en.wikipedia.org/wiki/Morse\\_potential](http://en.wikipedia.org/wiki/Morse_potential)
- [11] E. Gibb *et al.* *An Inventory of Interstellar Ices toward the Embedded Protostar W33A*. The Astrophysical Journal, 536, 347-356 (2000).
- [12] K. Isokoski *et al.* *Porosity and thermal collapse measurements of H<sub>2</sub>O, CH<sub>3</sub>OH, CO<sub>2</sub>, and H<sub>2</sub>O:CO<sub>2</sub> ices*. Phys. Chem. Chem. Phys., 2014, 16, 3456
- [13] Wikipedia: "Thin-film interference". Visited: 24-11-2014.  
[http://en.wikipedia.org/wiki/Thin-film\\_interference](http://en.wikipedia.org/wiki/Thin-film_interference)
- [14] S.O. Kasap, (2001). *Optoelectronics and Photonics: Principles and Practices*. (First edition - pp. 1-27). Prentice Hall, ISBN: 0-201-61087-6
- [15] W.R.M Rocha *et al.* *Determination of optical constants n and k of thin films from absorbance data using Kramers-Kronig relationship*. Spectrochimica Acta Part A: Molecular and Biomolecular Spectroscopy, Volume 123, 5 April 2014, Pages 436-446

- [16] J.-B. Bossa *et al.* *Porosity measurements of interstellar ice mixtures using optical laser interference and extended effective medium approximations*. *Astronomy & Astrophysics*, Volume 561, A136, January 2014.
- [17] J.H. Blankespoor, (2010). *Inleiding tot de toegepaste statistiek*. ThiemeMeulenhoff, ISBN: 978 90 06 95230 8.

## Appendix A

# Traineeship assignment description

A recent study performed in the Sackler Laboratory for astrophysics at Leiden Observatory has shown that measuring the refractive index of a porous ice mixture in the visible also allows to quantify its porosity. In the current traineeship, we propose to investigate a similar study by measuring the mid-infrared optical constants of different interstellar ice analogues. Most of our knowledge of ice composition is derived from infrared observations. However, ice structure and ice morphology are still open questions. From the infrared spectra recorded in the laboratory, it is possible to extract the wavelength dependent optical constants. From these optical constants, one can also extract the absolute band strengths, which are useful tools for astronomers to determine the ice composition in various astronomical environments. Experiments in Leiden will be performed on ice samples deposited on a cold substrates (30 K) inside high vacuum ( $10^{-8}$  Torr) cryogenic chambers capable of simulating the harsh physical conditions in space. Fourier transform infrared spectroscopy in transmission mode will be used as an analytical tool. Laser optical interferences will be conducted to measure with high precision the ice thicknesses during the different ice depositions. A program based on Fresnel equations and an iterative fitting procedure will be used to determine the real and imaginary part of the intrinsic optical constants in the mid infrared of pure and compact ices with known thicknesses. Finally, effective medium approximations will use these data to calculate and compare effective optical constants in the mid infrared of porous, binary and ternary composite ice materials as a function of wavenumber and porosity or abundances.

# Appendix B

## Python programs

In this chapter the different written Python programs are given, including a short explanation of each program.

### B.1 Min-Max

To determine the peak positions, a program is written which splits the interference signal peaks (see Fig. 2.8) into separate peaks. Because of the signal noise, the program shaves off values of the peaks, until multiple neighbouring and similar values are found (see Fig. B.2). The program then takes the median of these values, which is returned as the position of a peak. The advantage of this method over a smoothing function, is that there is no shift or lowering of the signal resolution with this method.

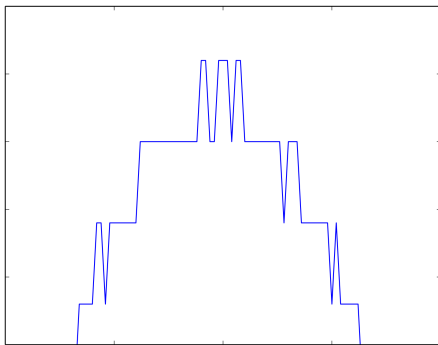


Figure B.1: A typical interference signal peak, measured by the photodiode. Note the noise in the signal.

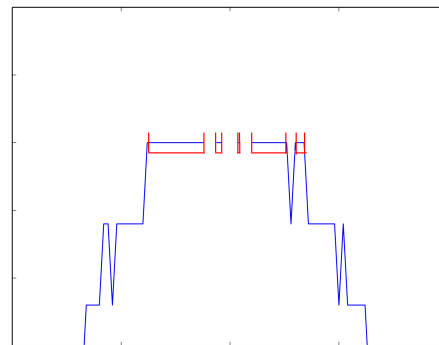


Figure B.2: The program shaves off the narrow signal spikes, until a broad enough spike is found. The red bracelets indicate the broadness the program is looking for.

```
1 import numpy as np
2 import matplotlib.pyplot as plt
3 from matplotlib import rcParams
4 import math # this is a standard python module, which enables working with
    trigonometric functions (sin, cos, pi, etc.)
```

```

5
6 path = '/home/fransen/Desktop/Coen/20140908/Time_ch1.txt'
7 starting_time_deposition = 16000 #timevalue at which the deposition is started
8
9 balance_line_value = 0.4          #balance line
10 step_size_minimum = 10 #minimum step size required for next intersection
    selection for balance_line_value
11 amount_peaks = 8 #amount of peaks used for calculation (minimums and maximums
    in measurement)
12 min_width_real_peak = 2 #required width of the min/max peak
13 refractive_index_sample = 1.285 #1.285 for pure methane at 30K. 1.3 for pure
    water at 30K. 1.3040 for H2O:CH4 (2:1) mix at 30 K (background)
14
15 plot0 = 1 #If this value is set to 1: plot unmanipulated data. If this value
    is 0: no plot.
16 plot1 = 0 #If this value is set to 1: plot shifted data (removed everything
    before the start time of deposition and shifted).
17 plot2 = 0 #If this value is set to 1: plot individual (cut-out) half wave. If
    this value is 0: no plot.
18 plot3 = 0 #If this value is set to 1: plot individual half wave (shifted
    downwards on the y-axis, absolute value). If this value is 0: no plot.
19 plot4 = 0 #If this value is set to 1: plot the unmanipulated data, but with
    lines through the selected local minima and maxima.
20         #The 'balance_line' is also plotted. This line is used to
            cut up the half waves. If this value is 0: no plot.
21 plot5 = 0 #If this value is set to 1: plot calculated ice thicknesses for each
    minimum and maximum, with the calculated linear line and formula.
22         #If this value is 0: no plot.
23
24 writetxt = 0 #If this value is set to 1: write the timevalue of the local
    minimum and maximum to .txt file
25         #If this value is 0: no .txt file
26 writetxt2 = 0 #If this value is set to 1: write the timevalue and the
    corresponding calculated ice thickness to .txt file
27         #If this value is 0: no .txt file
28 writetxt3 = 0 #If this value is set to 1: write the time from peak to peak, to
    .txt file
29         #If this value is 0: no .txt file
30
31 data_numpy = np.genfromtxt(path, delimiter=',')
32
33 if plot0 == 1: #plots untreated data
34     plt.plot(data_numpy[:,0], data_numpy[:,1])
35     plt.show()
36
37 pos_begin_dep = np.abs(data_numpy[:,0] - starting_time_deposition).argmin()
38 data_numpy = data_numpy[(pos_begin_dep):,:]
39 data_numpy[:,0] = data_numpy[:,0] - starting_time_deposition #subtract the
    starting time
40
41 if plot1 == 1: #plots the data with the starting time subtracted

```

```

42     plt.plot(data_numpy[:,0], data_numpy[:,1], )
43     plt.ylabel('Photodiode_signal_(V)')
44     plt.xlabel('Time_(s)')
45     plt.show()
46
47 #the following cuts up the data in separate peaks
48 data_sort = (data_numpy[:,1] > balance_line_value)
49 data_sort_value = data_sort.astype(np.int)
50 data_sort_diff = np.diff(data_sort_value)
51 begin_half_wave = (data_sort_diff== -1)
52 end_half_wave = (data_sort_diff==1)
53 begintimes = data_numpy[:,0][begin_half_wave].tolist()
54 endtimes = data_numpy[:,0][end_half_wave].tolist()
55
56 if len(begintimes) != len(endtimes):
57     y=(data_numpy[-1,0])
58     endtimes.append(y)
59
60 times = []
61 element = 0
62
63 while len(begintimes + endtimes) != len(times):
64     times.append(begintimes[element])
65     times.append(endtimes[element])
66     element = element +1
67
68 times_numpy = np.asarray(times)
69 times_diff = np.diff(times_numpy).tolist()
70
71 element2 = 1
72 times2=[]
73
74 times2.append(times[0])
75
76 #the following checks to see if the separate peaks are real peaks ,
77 #instead of small selections (few datapoints) jumping around the line used to
    cut the data into separate peaks (due to noise)
78 while element2 != len(times_diff):
79     if times_diff[element2-1] > step_size_minimum:
80         times2.append(times[element2])
81         element2 = element2 +1
82         continue
83
84     else:
85         element2 = element2 +1
86         continue
87
88 times2.append(times[-1])
89
90 if len(times2) != (amount_peaks+1):
91     del times2[amount_peaks+1:]

```

```

92
93 times2_repeat_values_except_first_last = np.repeat(times2, 2)[1:-1]
94 times2_repeat_values_reshaped = np.reshape(
    times2_repeat_values_except_first_last, (amount_peaks, 2))
95
96 list_timeranges = []
97
98 for timerange in times2_repeat_values_reshaped: #extracts the photodiode
    signal for each cut up peak
99     position_begin_half_wave = np.where(data_numpy[:,0] == timerange[0])
100     position_endtime_half_wave = np.where(data_numpy[:,0] == timerange[1])
101
102     half_wave_time_values = data_numpy[position_begin_half_wave[0]:
        position_endtime_half_wave[0],:]
103
104     list_timeranges.append(half_wave_time_values)
105
106
107 list_min_max_times = []
108
109 #the following shaves the narrow spikes (due to noise) off the cut up peaks,
110 #until a satisfying broadness is found, then takes the median of this
111 for timerange in list_timeranges:
112
113     if plot2 == 1:
114         time = [x[0] for x in timerange]
115         voltage = [x[1] for x in timerange]
116         plt.plot(time, voltage)
117         plt.show()
118
119     test_array = np.array(timerange[:,1])
120     test_array_substract = test_array - balance_line_value
121     array_insert_abs = np.abs(test_array_substract)
122     array_insert = np.insert(array_insert_abs, 0, 0)
123     max_value = np.max(array_insert_abs)
124     location_max = (array_insert_abs == max_value).astype(np.int)
125     where_max = np.diff(location_max)
126     start_false_peaks = np.where(where_max == 1)
127     end_false_peaks = np.where(where_max == -1)
128     start_false_peaks_conc = np.concatenate(start_false_peaks)
129     end_false_peaks_conc = np.concatenate(end_false_peaks)
130     stacked_false_peaks = np.vstack((start_false_peaks, end_false_peaks))
131     stacked_false_peaks = np.rot90(stacked_false_peaks, -1)
132     stacked_false_peaks = np.fliplr(stacked_false_peaks)
133     stacked_false_peaks_diff = np.diff(stacked_false_peaks)
134     stacked_false_peaks_diff_conc = np.concatenate(
        stacked_false_peaks_diff)
135     timerange_copy = array_insert_abs
136
137     for peak_width, peak_position in zip(stacked_false_peaks_diff_conc
       [:, -1], start_false_peaks_conc[:, -1]):

```

```

138         delete_range = np.arange(peak_position, (peak_position +
139             peak_width + 1))
140         if peak_width < min_width_real_peak:
141             timerange_copy = np.delete(timerange_copy,
142                 delete_range, 0)
143
144     if plot3 == 1:
145         time = [x for x in timerange_copy]
146         plt.plot(time)
147         plt.show()
148
149     max_value_real_peak = np.max(timerange_copy)
150     location_max_value_real_peak = np.where(max_value_real_peak ==
151         array_insert_abs)
152     time_max_value_real_peak = timerange[:,0][location_max_value_real_peak
153         ]
154     time_max_value_real_peak_median = np.median(time_max_value_real_peak)
155     list_min_max_times.append(time_max_value_real_peak_median)
156
157 list_min_max_times_numpy = np.array(list_min_max_times)
158 list_min_max_diff = np.diff(list_min_max_times_numpy)
159 list_min_max_minus_starting_time = list_min_max_times_numpy
160
161 if plot4 == 1: #plots the unmanipulated data with lines through the selected
162     peak positions
163     time = [x[0] for x in data_numpy]
164     voltage = [x[1] for x in data_numpy]
165     plt.plot(time, voltage)
166     plt.plot([time[0], time[-1]], [balance_line_value, balance_line_value
167         ])
168     plt.plot([list_min_max_times, list_min_max_times], [0.2, 0.7])
169     plt.show()
170
171 #the following calculates the ice layer thicknesses for the calculated peak
172     positions
173     m = np.arange(0.5, ((0.5 * len(list_min_max_minus_starting_time))+0.5), 0.5)
174     thickness_ice = ((632.8*(10**-9))*m) / (2 * refractive_index_sample * math.cos
175         (math.asin((math.sin(45*(math.pi/180)))/refractive_index_sample)))
176     thickness_ice_nanometers = thickness_ice / (10**-9)
177     a, b = np.polyfit(list_min_max_minus_starting_time, thickness_ice_nanometers,
178         1)
179     linear_line = (a*list_min_max_minus_starting_time + b)
180
181 if plot5 == 1: #plots the linear equation
182     plt.plot(list_min_max_minus_starting_time, thickness_ice_nanometers, '
183         ro')
184     plt.plot(list_min_max_minus_starting_time, linear_line, 'k-')
185     plt.xlim([0.5 * list_min_max_minus_starting_time[0], (1.1 *
186         list_min_max_minus_starting_time[-1])])
187     plt.ylim([0, (1.1 * thickness_ice_nanometers[-1])])
188     plt.xticks(fontname="Times New Roman")

```

```

178     plt.yticks(fontname="Times New Roman")
179     plt.text(list_min_max_minus_starting_time[1], thickness_ice_nanometers
180             [-1], 'y=%s_x=%s' % (a,b), fontsize=15, fontname="Times New
181             Roman")
182     plt.ylabel('Layer_thickness_(nm)')
183     plt.xlabel('Time_(s)')
184     plt.show()
185
186 if writetxt == 1: #writes the peak times to a txt file
187     file = open('time_peaks.txt', 'a')
188     file.write(path)
189     file.write('\n')
190     for item in list_min_max_minus_starting_time:
191         file.write("%s\n" % item)
192     file.write('\n\n')
193
194 if writetxt2 == 1: #writes the peak times with calculated ice layer
195     thicknesses to a txt file
196     file = open('time_thickness_20141126.txt', 'a')
197     file.write(path)
198     file.write('\n')
199     for time, thickness in zip(list_min_max_minus_starting_time,
200                               thickness_ice_nanometers):
201         file.write("%s, %s\n" % (time, thickness))
202     file.write('\n\n')
203
204 if writetxt3 == 1: #writes the time_peakpeak to a txt file
205     file = open('stepsize_peak_peak.txt', 'a')
206     file.write(path)
207     for timestep in np.diff(list_min_max_minus_starting_time):
208         file.write("%s\n" % (timestep))
209     file.write('\n')

```

## B.2 Sigma-calculator

For the calculation of the standard deviation in the linear regression, the following Python program is written:

```

1 import numpy as np
2 import csv
3 import matplotlib.pyplot as plt
4 from matplotlib import rcParams
5
6 path = '/home/fransen/Desktop/Results_python/CH4/time_thickness_test.txt'
7
8 data_numpy = np.genfromtxt(path, delimiter=',')
9 data_numpy = data_numpy[data_numpy[:,0].argsort()]
10
11 list_time = data_numpy[:,0]
12 list_thickness = data_numpy[:,1]

```

```

13
14 amount_h_measurements = len(list_time)
15
16 sum_xi_square = np.sum((list_time)**2)
17
18 sum_yi_square = np.sum((list_thickness)**2)
19
20 average_x = np.average(list_time)
21
22 average_y = np.average(list_thickness)
23
24 sum_xy = np.sum(list_time * list_thickness)
25
26 corr = (sum_xy - (amount_h_measurements * average_x * average_y)) / (((
    sum_xi_square - (amount_h_measurements * (average_x ** 2))) * (sum_yi_square
    - (amount_h_measurements * (average_y ** 2)))) ** 0.5)
27
28 a, b = np.polyfit(list_time, list_thickness, 1)
29
30 linear_line = (a * list_time + b)
31
32 SSE = np.sum((data_numpy[:, 1] - (a * data_numpy[:, 0] + b)) ** 2)
33
34 mean_square_error = (SSE / (amount_h_measurements - 2)) ** 0.5
35
36 sigma_b = mean_square_error * (((1.0 / amount_h_measurements) + ((average_x ** 2) / (
    np.sum((list_time - average_x) ** 2)))) ** 0.5)
37
38 sigma_a = mean_square_error * ((1 / np.sum((list_time - average_x) ** 2)) ** 0.5)
39
40 timerange = np.arange(0, (1.1 * np.max(list_time)), 1)
41
42 plt.plot(list_time, list_thickness, 'ro', label='combined_dataset')
43 plt.plot(list_time, linear_line, 'k-', label='linear_regression')
44
45 plt.xlim([0.5 * np.min(list_time), (1.1 * np.max(list_time))])
46 plt.ylim([0, (1.1 * np.max(list_thickness))])
47
48 plt.xticks(fontname="Times New Roman")
49 plt.yticks(fontname="Times New Roman")
50
51 plt.text(np.min(list_time), 0.85 * np.max(list_thickness), '$y_{\text{min}} = 0.3f_{\text{min}} + 0.0f_{\text{min}}$
    \n $r = 0.3f_{\text{min}}$ \n $\sigma_{\text{a}} = 0.3f_{\text{min}}$ \n $\sigma_{\text{b}} = 0.0f_{\text{min}}$' % (a, b, corr,
    sigma_a, sigma_b), fontsize=15, fontname="Times New Roman")
52
53 plt.legend(loc = 4)
54
55 rcParams['axes.labelsize'] = 10
56 rcParams['xtick.labelsize'] = 10
57 rcParams['ytick.labelsize'] = 10
58 rcParams['legend.fontsize'] = 10

```

```

59
60 plt.ylabel('Thickness_(nm)')
61 plt.xlabel('Time_(s)')
62
63 #plt.savefig('fig_time_thickness_linear_combined_CH4.png', dpi=300)
64
65 plt.show()

```

### B.3 NK-calculator

Since the optical constants are wavelength dependent, the written Python program first has to equalize the optical constants for both H<sub>2</sub>O and CH<sub>4</sub>. Since the resolution is not always identical for the input files (optical constants of H<sub>2</sub>O and CH<sub>4</sub>), the program takes this into account by defining a list of wanted wavenumbers (for instance: 4000, 3998, 3996, ...), and selecting the optical constants closest to the wavenumber of the list. The associated optical constants are then used to calculate the effective optical constants for the mixture (see chapter 2.4).

```

1 import numpy as np
2 import csv
3 import matplotlib.pyplot as plt
4 import math
5 from sympy.solvers import solve
6 from sympy import Symbol
7 from sympy import nsolve
8 from sympy import sympify
9 from sympy import I
10 from sympy import *
11
12
13 NK_CH4 = np.genfromtxt('/home/fransen/Desktop/Results_python/NK/
    nk_CH4_30K_fixed.csv', delimiter=',')
14 NK_H2O = np.genfromtxt('/home/fransen/Desktop/Results_python/NK/
    nk_H2O_30K_fixed.csv', delimiter=',')
15
16 writetxt = 1 #writes txt file with epsilon_eff
17 writetxt2 = 1 #writes txt file with calculated n and k
18
19 upper_limit_wavenumber = 4000 #any wavenumber above this value is removed from
    the dataset, use 0 if no removal is needed
20 lower_limit_wavenumber = 7500 #any wavenumber below this value is removed from
    the dataset, use 0 if no removal is needed
21 wanted_stepsize_wavenumber = 2 #the wanted wavenumber stepsize in the dataset
22
23 #the following creates the volume fractions to be used in the calculations
24 ratio_H2O_CH4 = 2
25 f_a = np.arange(.4, 0.5, 0.1)
26
27 f_b = ((1-f_a)/(ratio_H2O_CH4+1))*ratio_H2O_CH4
28 f_c = (f_b / ratio_H2O_CH4)
29
30 #the following removes any datapoints from outside the given range

```

```

31 #and solves for the possible different wavenumber resolution
32 wanted_wavenumbers = np.arange(lower_limit_wavenumber, (upper_limit_wavenumber
    +wanted_stepsize_wavenumber), wanted_stepsize_wavenumber)
33
34 list_selected_data_pos_CH4 = []
35
36 for wavenumber in wanted_wavenumbers:
37     closest_wavenumber_pos_CH4 = (np.abs(NK_CH4[:,0] - wavenumber)).
        argmin()
38     list_selected_data_pos_CH4.append(closest_wavenumber_pos_CH4)
39
40 NK_CH4_selected = NK_CH4[list_selected_data_pos_CH4]
41 NK_CH4_selected2 = np.array([wanted_wavenumbers, NK_CH4_selected[:,1],
    NK_CH4_selected[:,2]])
42
43
44 list_selected_data_pos_H2O = []
45
46 for wavenumber in wanted_wavenumbers:
47     closest_wavenumber_pos_H2O = (np.abs(NK_H2O[:,0] - wavenumber)).
        argmin()
48     list_selected_data_pos_H2O.append(closest_wavenumber_pos_H2O)
49
50 #the following changes the 'layout' of the data, so that it can be used in the
    following for-loops
51 NK_H2O_selected = NK_H2O[list_selected_data_pos_H2O]
52 NK_H2O_selected2 = np.array([wanted_wavenumbers, NK_H2O_selected[:,1],
    NK_H2O_selected[:,2]])
53
54 CH4_selected_data_rot = np.rot90(NK_CH4_selected2, -1)
55 CH4_selected_data_flip = np.fliplr(CH4_selected_data_rot)
56
57 H2O_selected_data_rot = np.rot90(NK_H2O_selected2, -1)
58 H2O_selected_data_flip = np.fliplr(H2O_selected_data_rot)
59
60 CH4_selected_data_flip = CH4_selected_data_flip[np.logical_not(np.isnan(
    CH4_selected_data_flip[:,1]))]
61 CH4_selected_data_flip = CH4_selected_data_flip[np.logical_not(np.isnan(
    CH4_selected_data_flip[:,2]))]
62
63 H2O_selected_data_flip = H2O_selected_data_flip[np.logical_not(np.isnan(
    H2O_selected_data_flip[:,1]))]
64 H2O_selected_data_flip = H2O_selected_data_flip[np.logical_not(np.isnan(
    H2O_selected_data_flip[:,2]))]
65
66 #the following calculates the n and k values, for ranges of volume fractions (
    f_x)
67 #creates and writes txt files with volume fractions in title and n and k
    values in file
68 for f_a, f_b, f_c in zip(f_a, f_b, f_c):
69

```

```

70     for H2O, CH4 in zip(H2O_selected_data_flip , CH4_selected_data_flip):
71
72         CH4_N = CH4[1]
73         CH4_K = CH4[2]
74         H2O_N = H2O[1]
75         H2O_K = H2O[2]
76
77         epsilon_CH4 = (((CH4_N**2) - (CH4_K**2)) - (I*(2*CH4_N*CH4_K)))
78         epsilon_H2O = (((H2O_N**2) - (H2O_K**2)) - (I*(2*H2O_N*H2O_K)))
79
80         x = Symbol('x')
81         epsilon_eff = solve(( f_a*((1-x)/(1+2*x)) + f_b*((epsilon_CH4
            - x)/(epsilon_CH4 + 2*x)) + f_c*((epsilon_H2O - x)/(
            epsilon_H2O + 2*x))) - 0, x)
82
83         if writetxt == 1:
84             path = 'data_epsilon_eff_mix_fa_(%s)_ratio_(%s).txt' %
            (f_a, ((f_b/f_c)))
85             file = open(path, 'a')
86             file.write("%s,%s\n" % (H2O[0], epsilon_eff[-1]))
87
88         x = Symbol('x')
89         y = Symbol('y')
90
91         result_NK = nsolve([((x**2)-(y**2)) - (re(epsilon_eff[-1])),
            (-2*x*y) - (im(epsilon_eff[-1]))], [x, y], [H2O_N, H2O_K])
92         print '\nN_eff:_', result_NK[0]
93         print 'K_eff:_', result_NK[1]
94         N = result_NK[0]
95         K = result_NK[1]
96
97
98         if writetxt2 == 1:
99             path = 'data_NK_eff_mix_fa_(%s)_ratio_(%s).txt' %(f_a ,
            ((f_b/f_c)))
100            #print path
101            file = open(path, 'a')
102            file.write("%s,%s,%s\n" % (H2O[0], result_NK[0],
            result_NK[1]))

```

## Appendix C

# Succeeding deposition spectra measurements

The original plan for acquiring the spectra of pure and compact (non porous)  $\text{H}_2\text{O}$  and  $\text{CH}_4$ , was to measure multiple spectra for different ice layer thicknesses in a single experiment. This meant that the deposition was to be paused before a spectrum could be measured, so the deposited ice layer thickness was kept constant. It was, however, suspected that that when the front deposition was paused by closing two valves between the sample and the vacuum chamber, the residual gasses in the vacuum continued to deposit (background deposition) on the substrate (see Fig. C.1). To quantify the amount of background deposition during a deposition pause, a Python program was written.

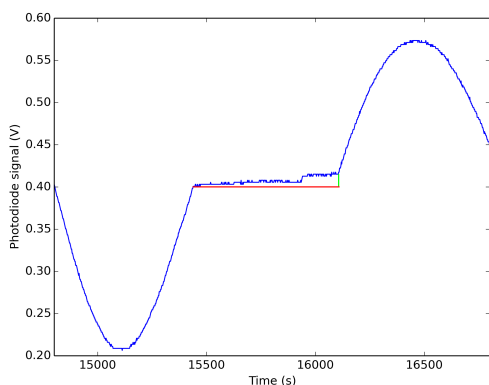


Figure C.1: The effect of pausing the deposition on the interference signal measured by the photodiode. The red marker indicates the photodiode signal increase.

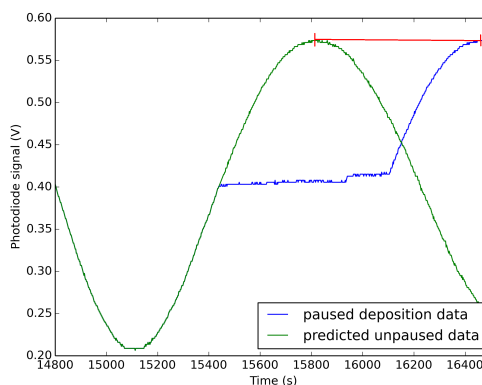


Figure C.2: The predicted peak position for an unpaused deposition. The red marker indicates the time difference between the real and predicted peak.

The small jump in the interference signal measured by the photodiode is due to the procedure of preparing for the continuation of the deposition (by opening one of the valves). To determine how much was deposited in this period, a Python program is written. The program first cuts out the deposition pause, and shifts the following peaks so that it connects with the last datapoint before the pause. This, however, does not allow for a smooth transition between the pre and post pause photodiode signal. By the use of Eq. 2.12, a prediction is made where the first following peak would be if the deposition was not paused (see Fig. C.2). The time difference between the real and predicted peak (red marker) is then calculated. From this value

the duration of the deposition pause is subtracted. This results in a difference of  $20 \pm 3$  s, which indicates that the background deposition during the deposition pause equals  $20 \pm 3$  s at the normal deposition rate. To validate the calculation, the photodiode datapoints during the pause are removed and the data is shifted back. The data is then reshifted forward for 20 s, resulting in a confirming fit (see Fig. C.3).

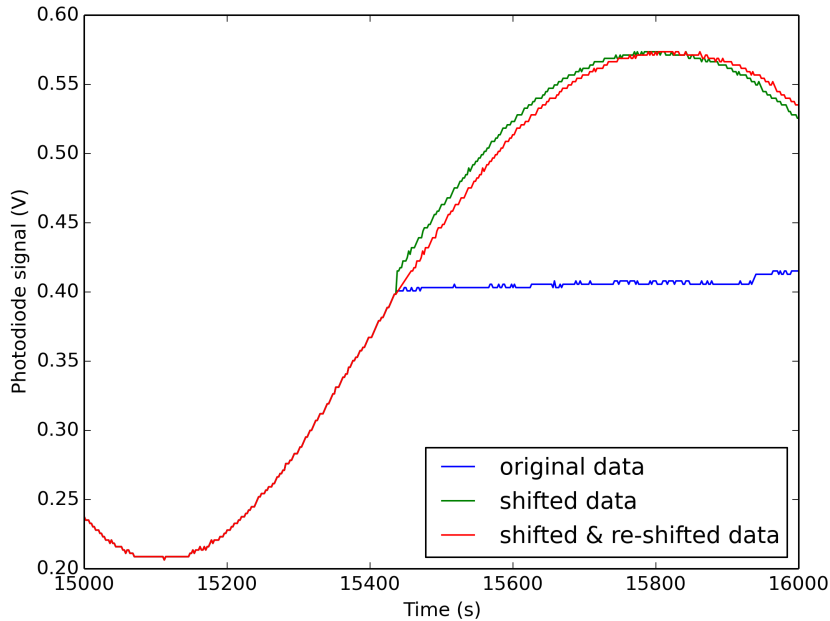


Figure C.3: The effect of shifting and re-shifting the photodiode signal data.

However, the procedure of pausing and continuing the deposition demanded for the hose connecting the sample bulb with the vacuum chamber to be pumped. If this was not done, the jump in photodiode signal (as indicated by the light green marker in Fig. C.1) would increase greatly. The deposition rate is not only determined by the setting, but also by the pressure on the entry side of the needle valve. Hence it was decided to quantify the change in deposition rate, since pumping the hose decreases the pressure in the sample bulb and the hose itself (see Fig 3.1). This was done by pausing and continuing the deposition once and twice. After the pauses, the deposition was continued normally and the deposition rate determined by the use of the method described in chapter 2.3. From this it was concluded that the variation in the deposition rate increases too much after multiple deposition pauses (see Fig. C.4). To prevent this effect from adding extra uncertainty, it was decided that a better approach would be to measure each spectrum for each ice layer thickness on different experiments (days).

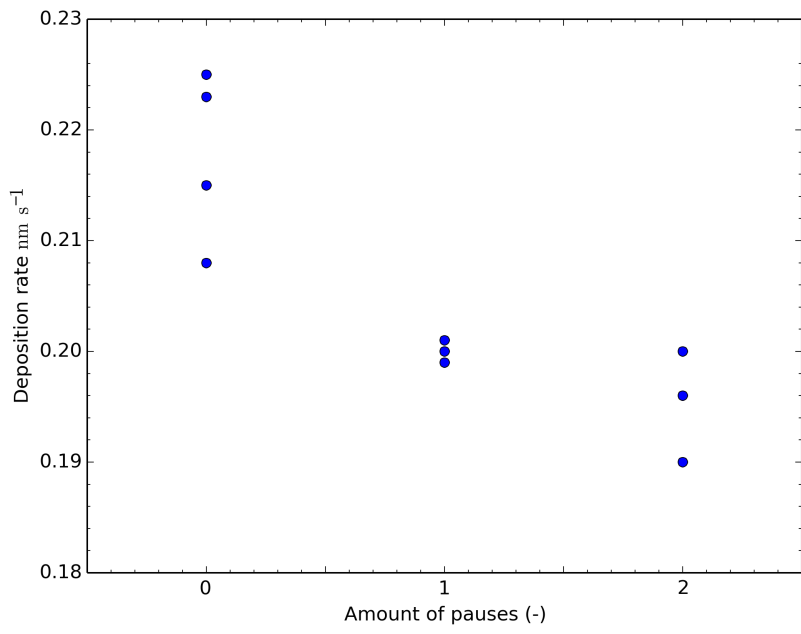


Figure C.4: The calculated deposition rates after 0, 1 and 2 pauses.